Water Resources Research

RESEARCH ARTICLE
10.1029/2017WR021764

Glacier Recession and the Response of Summer Streamflow in the Pacific Northwest United States, 1960–2099

Chris Frans[1,2], Erkan Istanbulluoglu[2], Dennis P. Lettenmaier[3], Andrew G. Fountain[4], and Jon Riedel[5]

[1]U.S. Army Corps of Engineers, Seattle, WA, USA, [2]Department of Civil and Environmental Engineering, University of Washington, Seattle, WA, USA, [3]Department of Geography, University of California, Los Angeles, CA, USA, [4]Department of Geology, Portland State University, Portland, OR, USA, [5]North Cascades National Park, U.S. National Park Service, Sedro-Woolley, WA, USA

Key Points:
- Spatial and temporal patterns of glacier retreat and hydrological response are illustrated for the Pacific Northwest United States 1960–2099
- The relative contribution of glacier melt in space and time is characterized at the basin and channel network scale
- The response of summer streamflow to glacier recession varies greatly with respect to local climate

Correspondence to:
C. Frans,
chris.d.frans@usace.army.mil

Citation:
Frans, C., Istanbulluoglu, E., Lettenmaier, D. P., Fountain, A. G., & Riedel, J. (2018). Glacier recession and the response of summer streamflow in the Pacific Northwest United States, 1960–2099. *Water Resources Research*, *54*. https://doi.org/10.1029/2017WR021764

Received 1 SEP 2017
Accepted 9 AUG 2018
Accepted article online 16 AUG 2018

Abstract The Pacific Northwest is the most highly glacierized region in the conterminous United States (858 glaciers; 466 km^2). These glaciers have displayed ubiquitous patterns of retreat since the 1980s mostly in response to warming air temperatures. Glacier melt provides water for downstream uses including agricultural water supply, hydroelectric power generation, and for ecological systems adapted to cold reliable streamflow. While changes in glacier area have been studied within the region over an extended period of time, the hydrologic consequences of these changes are not well defined. We applied a high-resolution glacio-hydrological model to predict glacier mass balance, glacier area, and river discharge for the period 1960–2099. Six river basins across the region were modeled to characterize the regional hydrological response to glacier change. Using these results, we generalized past and future glacier area change and discharge across the entire Pacific Northwest using a k-means cluster analysis. Results show that the rate of regional glacier recession will increase, but the runoff from glacier melt and its relative contribution to streamflow display both positive and negative trends. In high-elevation river basins enhanced glacier melt will buffer strong declines in seasonal snowpack and decreased late summer streamflow, before the glaciers become too small to support streamflow at historic levels later in the 21st century. Conversely, in lower-elevation basins, smaller snowpack and the shrinkage of small glaciers result in continued reductions in summer streamflow.

1. Introduction

Over the past several decades pervasive patterns of glacier mass loss have been observed in glacierized regions across the globe in response to warming air temperatures (e.g., DeVisser & Fountain, 2015; Marzeion et al., 2014; Ohmura, 2011). The mass loss is expressed as increased alpine streamflow compared to ice-free watersheds. However, elevated streamflow cannot be maintained as the glaciers shrink; therefore, under conditions of a trend in warming air temperatures, glacial runoff increases initially and once the glacier area has been reduced sufficiently glacial runoff decreases as the glacier further recedes (Huss & Hock, 2018; Jansson et al., 2003; Moore et al., 2009). Alpine runoff is not only affected by glacial melt but also rainfall and other factors, which respond to increasing temperature, including seasonal snow accumulation and melt, evapotranspiration (Frans et al., 2015). The relative importance of each of these factors varies as a function of changing local- and regional-scale climate, initial relative glacier cover, and the timescale of interest (annual and seasonal).

The hydrological response of watersheds to glacier recession over decades is poorly understood due to the limited number of observations in alpine environments and challenges posed by difficulties in capturing processes within the nonglacierized portions of the watershed. Recently, observational and modeling efforts have been developed and applied to further our understanding of these processes (e.g., Nolin et al., 2010; Ragettli et al., 2015; Van Beusekom & Viger, 2016; Huss & Fischer, 2016). These efforts have largely been focused on individual highly glacierized river basins (e.g., Finger et al., 2012; Jost et al., 2012; Ragettli et al., 2015) and more recently at the global scale (e.g., Huss & Hock, 2018; Schaner et al., 2012). Less attention has been given to regional hydrological responses to warming using detailed analyses of both glacierized and nonglacierized portions of watersheds outside of the High Mountain Asia and Andes regions (e.g., Baraer et al., 2012; Fernández & Mark, 2016; Immerzeel et al., 2013; Lutz et al., 2014).

Using a regional glacier dynamics model (GDM), Clarke et al. (2015) predict changes in glacier mass, area, and melt across western Canada over the period of 1980–2100. Their work represents a major advance in the prediction of future glacier change at a regional scale; however, their analysis is limited to glaciers and does not consider the role of hydrologic processes in the nonglacierized parts of the watershed. Stahl and Moore (2006) analyze streamflow records across western Canada and found statistically significant decreasing late summer discharge in basins with extensive glacier cover, confirming pervasive changes in streamflow in partially glacierized watersheds. However, their statistical analyses provide limited insights into the mechanisms behind the changes and do not attribute the changes to specific sources such as snowmelt, glacier melt, or both.

The Pacific Northwest (PNW), defined here as including Washington, Oregon, Idaho, and Montana (west of the continental divide), is populated by about 858 glaciers totaling 466 km^2 (Fountain et al., 2017). Glacier meltwater is important for water supply and hydroelectric power generation (Tangborn, 1984; Schaefli et al., 2007) and for maintaining sufficient in-stream flows for fisheries and other ecological functions of riverine systems. Furthermore, there are growing concerns about the potential risk of landslides and ecosystem succession following glacial recession (Moore et al., 2009; Strauch et al., 2018). Better understanding of these changes and assessing future implications require a glacio-hydrologic modeling approach, which is the basis for our study.

In this study we ask the following two related questions: (1) What is the current contribution of PNW glaciers to streamflow? (2) How will the interplay between warming and snow accumulation-melt dynamics influence glacial contribution to low flows and the timing of a peak glacier contribution? To address these questions we generalize spatial and temporal patterns of glacier retreat over the PNW region, characterize the glacier contribution to streamflow across channel networks, and predict how hydrological response to glacier recession varies within the region. Glacier and streamflow response are modeled using the Distributed Hydrology Soil Vegetation Model (DHSVM) glacio-hydrological model (Frans et al., 2015; Naz et al., 2014), driven by regional gridded hydroclimate data. Spatially distributed observations of glacier mass and area and streamflow are used for model calibration and confirmation. We apply this approach to six partially glacierized watersheds within temperate northern latitudes (45–49°) of the PNW that represent a range of elevations and climatic gradients. We then postprocess these results in a macroscale statistical model to make general inferences of future glacier change for the region.

2. Study Region

Within the PNW we focus on the Olympic Range in Washington and the Cascade Range in Oregon and Washington extending as far south as Mount Hood in Oregon (Figure 1). The major topographic feature of the region is the Cascade Range, which acts as a north-south orographic barrier that strongly influences the longitudinal distribution of the region's precipitation. The Cascade Range and the proximity of the Pacific Ocean define two major climate zones: maritime to the west with a maritime-continental transition climate to the east. The maritime climate on the west side of the Cascade Range is characterized by mild air temperatures and high amounts of precipitation that mostly occurs from late fall to early spring. The continental climate on the east side is much drier and colder in winter and warmer in summer. Interannual to decadal variations in sea surface temperatures associated with the El Niño-Southern Oscillation (ENSO) phenomenon and the decadal Pacific Decadal Oscillation (PDO) modulate long-term variations the region's winter climate (Mantua et al., 1997).

Glaciers are commonly found in the region, with relatively intense glaciation in northern Washington decreasing to the south, where in Oregon the glaciers are limited to the high-elevation stratovolcanoes. Over the last century glacier area has been shrinking as much as 50% in the North Cascade Range (Dick, 2013) to as little as 22% on Mount Rainier (Nylen, 2004). Glacier area in the Olympic Range in the northwestern corner of Washington decreased 52% (Riedel et al., 2015). Although long-term changes in glacier area have been documented using aerial and satellite imagery; the hydrological consequences of these changes are not well defined in the PNW.

To characterize glacio-hydrological responses and its variability across the region, we selected six river basins that span the region (Figure 1 and Table 1). The drainage areas of these basins range from 270 to 879 km^2 with glacier area cover ranging from <1 to 13.6% of the basin area. Mean annual precipitation of all of the

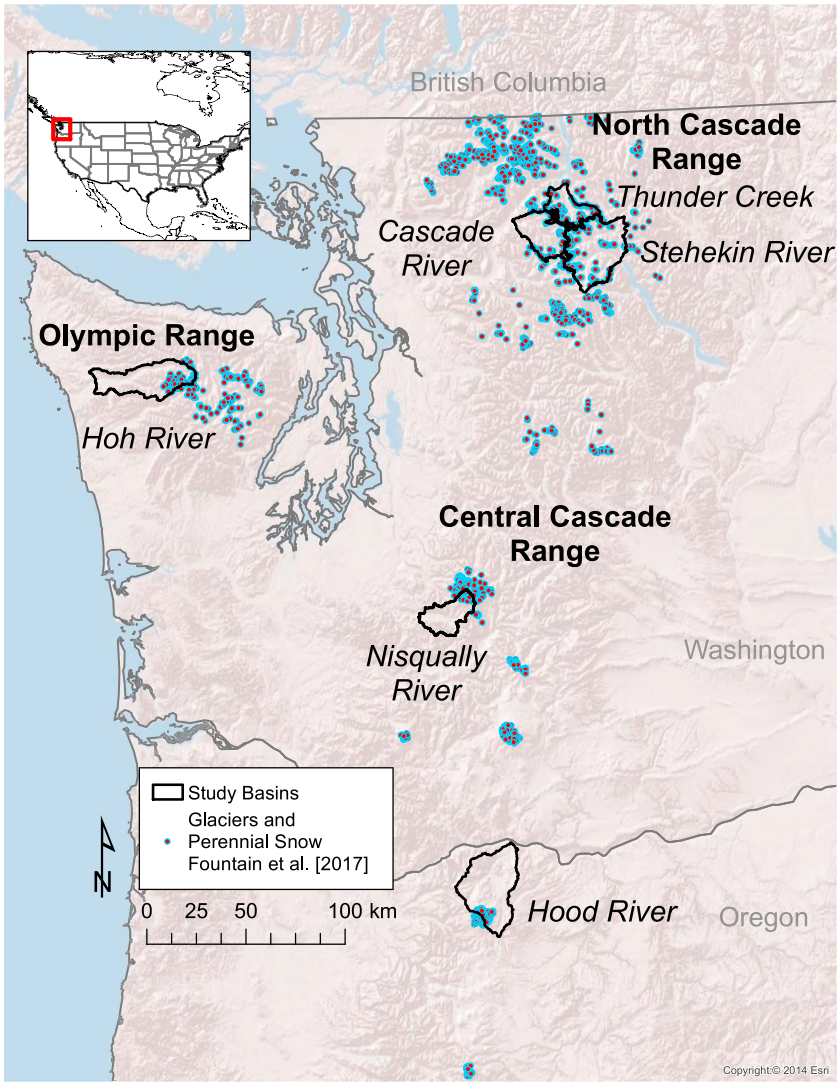

Figure 1. Location of river basins included in the regional analysis. The basin drainage areas are defined with black lines. Markers for glaciers and perennial snowfields (Fountain et al., 2017) indicate the centroid of the feature.

basins ranges from 1,700 to 3,800 mm (Daly et al., 1994). End-member basins with respect to climate are the Hoh River basin on the maritime west slopes of the Olympic Range with high precipitation (up to ~6,500-mm mean annual precipitation) resulting in the lowest elevation glaciers (~1,100 m) and the Nisqually River basin

Table 1
Characteristics of the River Basins Included in the PNW Regional Analysis

Basin	Drainage area (km^2)	Mean precip. (mm/yr)	Max elev. (m)	Mean elev. (m)	Glacier area (km^2)	Glacier cover (%)
Thunder	270	2,220	2,740	1,570	36.8 (1960[a])–32.1 (2010[a])	13.6–11.9
Cascade	440	2,370	2,660	1,270	16.3 (1960[a])–11.9 (2010[c])	3.7–2.7
Stehekin	830	1,700	2,110	1,630	24.2 (1960[a])–18.7 (2010[b])	2.9–2.3
Nisqually	360	2,300	4,380	1,240	26.4 (1913[d])–18.2 (2009[d])	7.3–5.0
Hoh	640	3,830	2,370	775	23.7 (1985[e])–18.0 (2009[b])	3.7–2.8
Hood	880	1.800	3,400	927	6.7 (1904[f])–4.6 (2004[f])	<1

Note. The sources of glacier area data are listed below the table.
[a]Dick, 2013. [b]Granshaw and Fountain (2006). [c]Landsat Normalized Difference Snow Index derived. [d]Andrew Fountain, www.glaciers.pdx.edu. [e]Spicer, 1986. [f]Jackson and Fountain (2007).

Table 2
Data Utilized as Model Input and for Model Calibration and Verification

Data	Description	Source
Model input		
Digital elevation model	Shuttle Radar Topography Mission (SRTM), 30 m	http://www.opentopography.org/
Soil texture	NRCS STATSGO2	http://www.nrcs.usda.gov/
Vegetation	National Land Cover Database (NLCD 2011), 30 m	http://www.mrlc.gov/nlcd2011.php
1981–2010 precipitation normals	PRISM Climate Group, 800 m	http://www.prism.oregonstate.edu/
Historical meteorological data	Livneh et al. (2013), 1/16 degree	http://maca.northwestknowledge.net
Future meteorological data	MACA Downscaled CMIP5 GCM Output, 1/16°	http://maca.northwestknowledge.net
Model calibration/verification		
Glacier area	Glacier Research at Portland State University	Dick (2013); Nylen (2004); Spicer (1986)
Glacier area	Landsat CDR NDSI derived Snow/Ice Extent	http://earthexplorer.usgs.gov/
Glacier mass balance	National Park Service	Riedel and Larrabee (2011b)
Glacier mass balance	United States Geological Survey	http://www.usgs.gov/climate_landuse/clu_rd/glacierstudies/default.asp
Glacier mass balance	University of Washington	http://earthweb.ess.washington.edu/Glaciology/projects/blue_glac/mass_balance.htm
Discharge	United States Geological Survey Stream Gauging	http://waterdata.usgs.gov/nwis/
Snow water equivalent	NRCS Snow Telemetry (SNOTEL)	http://www.wcc.nrcs.usda.gov/snow/
1981–2010 temperature normals	800 m, PRISM Climate Group	http://www.prism.oregonstate.edu/

Note. CMIP5, Coupled Model Inter-Comparison Project 5; GCM, global climate model; MACA, Multivariate Adaptive Constructed Analogs; NDSI, Normalized Difference Snow Index; PRISM, Parameter elevation Regression on Independent Slopes Model.

whose headwaters extend to the highest elevations in the region (~4,400 m) on the southern flanks of Mount Rainier in the maritime climate. Three basins that are positioned near the crest of the Cascades represent a gradation of the transition from maritime to more continental climate: Thunder Creek in the North Cascade Range, the most heavily glacierized in this study, and the Cascade and Stehekin river basins.

3. Approach

3.1. Glacio-hydrological Model

We used the DHSVM (Wigmosta et al., 1994; Wigmosta et al., 2002) coupled with the GDM of Clarke et al. (2015) to simulate glacio-hydrological processes in each of the six river basins. DHSVM has been widely applied in the mountainous western United States in snow hydrology studies (e.g., Cristea et al., 2014; Jost et al., 2009) and in climate and land cover change applications (e.g., Cuo et al., 2011; Elsner et al., 2010). The GDM is required to evolve the distribution of glacier ice in response to snow accumulation and snow/ice ablation (glacier mass balance). It is based on the shallow ice approximation of the equations governing ice deformation (Cuffey & Paterson, 2010) and sliding to simulate the lateral movement of ice as described in Jarosch et al. (2013) and Clarke et al. (2015). Several changes have been made to DHSVM to link with GDM explained in detail by Naz et al. (2014). A glacier ice layer is added to the bottom of a snowpack layer in the snowpack energy balance model to represent glacier ice accumulation, ablation, and mass balance. The general framework of the coupling is that snow and ice accumulation and melt are simulated in the subdaily algorithms of the hydrological model, and at the end of each month these fluxes are summed to produce net changes in glacier mass. This mass change is then used to force the GDM, which in turn updates the thickness of glacier ice in each model grid cell as ice flows in response to slope, curvature, and ice thickness. Melting snow and glacier ice enters the soil column of the respective grid cell and is then routed through the watershed following the subsurface and surface flow modeling schemes of DHSVM (Wigmosta et al., 1994; Wigmosta et al., 2002). Recently, the effects of supraglacial debris on surface energy balance for glaciers was incorporated in the ice ablation algorithms of the DHSVM snowmelt model to study glaciers with debris cover (Frans et al., 2016). In this study we also incorporate an algorithm in DHSVM that redistributes snow from avalanching (Bernhardt & Schulz, 2010), which can be a significant source of mass accumulation for some glaciers and impact snowmelt discharge patterns (Freudiger et al., 2017).

We implemented both GDM and DHSVM at spatial resolutions of 50 m. We resampled (bilinear) hydrological model parameters (e.g., elevation, soil, and vegetation) from their native resolution to 50 m. The sources of geospatial data used are listed in Table 2.

Table 3
Optimal Parameters Found Through Mass Balance Calibrations of Individual Glaciers

Glacier	Basin	P. Multi	Tlapse (°C/km)	MaxSnow α	Glacier α	Rl (mm)
South Cascade	Cascade	1.00	−8.6	0.88	0.36	0.91
North Klawatti	Thunder	0.99	−9.8	0.88	0.33	1.50
Sandalee	Stehekin	3.47	−7.2	0.9	0.42	2.02
Nisqually	Nisqually	1.01	−4.4	0.81	0.32	7.17
Blue	Hoh	1.34	−6.2	0.87	0.39	3.81

Note. P. Multi is the precipitation multiplier, Tlapse is the air temperature lapse rate (constant), MaxSnow α is the maximum albedo of snow used in temporal decay curves, Glacier α is glacier albedo, and Rl is the aerodynamic roughness length over snow and ice.

3.2. Model Forcing Data

For the historical glacio-hydrological simulations we used the gridded meteorological data set of (Livneh et al., 2013). These data consist of daily minimum (Tmin) and maximum (Tmax) air temperature at 2 m above ground level, precipitation, and wind speed at a spatial resolution of 1/16° (~6 km N-S). This data set is also the historical reference used in bias correcting and downscaling an ensemble of global climate model (GCM) outputs. The GCM models were selected based on the model skill rankings of Rupp et al. (2013), who evaluated output from the Coupled Model Inter-Comparison Project 5 (CMIP5) for the PNW. The Multivariate Adaptive Constructed Analogs (MACA) statistical methods (Abatzoglou & Brown, 2012) were used to downscale the CMIP5 data as part of the Integrated Scenarios of the Northwest Environment project (http://pnwcirc.org/projects/integrated-scenarios/). The combination of historical data and downscaled MACA future climate projections provided DHSVM forcing data for a 185-year period 1915–2099.

The algorithm for generating the historical data set used a constant temperature lapse rate (−6.5 ° km^{-1}C/° km) to interpolate Tmin and Tmax to 1/16° resolution from local weather stations (Livneh et al., 2013). We evaluated the effects of this assumption by comparing the local climatology of each grid cell with that of the Parameter elevation Regression on Independent Slopes Model (PRISM; Daly et al., 1994) 800-m resolution climatology resampled to 1/16°. In mountainous areas with high vertical relief and low station density, the Livneh et al. (2013) data were significantly colder than the PRISM 1981–2010 climate normals. At high elevations cold biases are pervasive throughout the year in Tmin and during winter months in Tmax (up to −8°C). To remove these biases, we corrected the Livneh et al. data using a delta method (e.g., Watanabe et al., 2012) for monthly Tmin and Tmax derived from the comparisons with the PRISM data:

$$T_{\mathrm{bc},i} = T_{\mathrm{Livneh},i} + \left(\overline{T}_{\mathrm{PRISM,month}} - \overline{T}_{\mathrm{Livneh,month}}\right) \quad (1)$$

where $T_{\mathrm{bc},\ i}$ is the bias corrected value of the daily historical temperature value of day, *i*. We used the differences between the PRISM climatological mean ($\overline{T}_{\mathrm{PRISM,month}}$) and the historical climatological mean ($\overline{T}_{\mathrm{Livneh,month}}$) for the corresponding month for bias correction. These bias corrections were applied to the future MACA downscaled data as well.

We temporally disaggregated the daily bias corrected meteorological data to a 3-hourly time interval using the Mountain Microclimate Simulation Model (MTCLIM) algorithms (Thornton & Running, 1999) as implemented in Bohn et al. (2013). To distribute these data spatially to the finer-resolution model domain (50 m), the centroid locations and the mean elevations of each 1/16° grid cell were used to estimate temperature at the 50-m model resolution using calibrated temperature lapse rates (section 3.4 and Table 3), the 50-m digital elevation model (DEM), and bilinear interpolation between centroids.

In contrast to air temperature, systematic differences between the Livneh et al. (2013) and PRISM data were not identified and bias correction was not applied. We spatially distributed precipitation from the centroid locations of the regional data sets to the 50-m model grid cell using PRISM precipitation normals as a template,

$$P_{x,y} = \left(\mathrm{PRISM}_{x,y,\mathrm{month}} / \mathrm{PRISM}_{x_{\mathrm{centroid}},y_{\mathrm{centroid}},\mathrm{month}}\right) \times P_{\mathrm{centroid}} \quad (2)$$

where the precipitation at a local 50-m grid cell ($P_{x,\ y}$) is calculated using the precipitation of the Livneh et al. 1/16°data (P_{centroid}) and the relationship between the local PRISM precipitation normal value for the

current month ($PRISM_{x,\ y,\ month}$) with the PRISM precipitation normal value for location of the centroid ($PRISM_{x_{centroid},y_{centroid},month}$). In this manner, we used the relative spatial patterns of PRISM to spatially distribute the coarser data. In DHSVM, shortwave radiation used in surface energy balance ice and snowmelt algorithms and in the calculation of evapotranspiration is distributed based on a solar geometry model that accounts for sloped surfaces and terrain shading for each 3-hr time interval of the day and month of the year (Wigmosta et al., 1994).

3.3. Observational Data

Confidence in model predictions depends in part on how well the model reproduces historical glaciological and hydrological variables such as glacier mass, glacier area, and streamflow. We used glacier mass observations to test the climate and energy balance algorithms of DHSVM for producing local glacier ice. Existing measurements of net glacier mass balance were obtained for the Nisqually, Thunder Creek, and Stehekin (Riedel & Larrabee, 2011a); the Cascade River (U.S. Geological Survey [USGS], Washington Water Science Center); and the Hoh River (Conway et al., 1999) basins.

Estimates of glacier area at discrete points in time were used to define the change in extent through the historical period and were compared against modeled glacier areas to confirm the coupled DHSVM-GDM model predictions. We used glacier area data based on historical aerial imagery and topographic maps compiled by the glacier research groups at Portland State University (Dick, 2013; Granshaw & Fountain, 2006; Nylen, 2004) and the National Park Service (Riedel et al., 2015). We relied on estimates of glacier area from Landsat satellite imagery for the end of the most recent decade (approximately 2010) in basins where these more rigorously compiled data were not yet available (Cascade, Stehekin, and Hoh). Landsat-based estimates used classifications of atmospherically corrected images using the Normalized Difference Snow Index (NDSI) methodology described in Burns and Nolin (2014). The Landsat images were chosen from dates at the end of the melt seasons of anomalously dry years (low winter precipitation and thin snowpack) to avoid confounding glacier areas with seasonal snow. The Landsat estimates were only used if other more robust observational data sets were unavailable. The data sources used to define glacier area for different periods of time are listed in Table 1.

Stream gages from the USGS (waterdata.usgs.gov/nwis/) were used to evaluate model predicted runoff patterns. Gauges were selected based on their proximity to glaciers and length of record.

3.4. Glaciological and Hydrological Calibration

The model calibration and the initialization of glacier masses were organized in three incremental steps: (1) Cryospheric calibration: calibration of climate and surface energy balance parameters that control the accumulation and ablation of snow and ice against observations for measured glaciers in each basin. This step is critical because snow dynamics control glacier mass and the volume and timing of spring and summer streamflow. (2) Glacier ice spin-up: First DHSVM is run to produce a spatially distributed mean annual mass balance of glacier ice, then the GDM is run over large timescales driven by this mass balance to form initial glacier conditions for modern-day simulations. This step aims to produce glacier ice mass extents consistent with historical extent observations. (3) Hydrological calibration: calibration of soil parameters to improve streamflow simulation using ranges of select soil parameters. These steps were followed for all basins except for the Hood River watershed where additional observational data required a slightly different procedure for calibration and testing (e.g., observations of subdebris ablation and geochemical sampling; Frans et al., 2016).

The parameters included for cryospheric calibration were air temperature lapse rate (constant throughout the year), a precipitation multiplier, maximum snow albedo used by snow albedo decay functions (Laramie & Schaake, 1972; Wigmosta et al., 2002), glacier ice albedo, and a constant for the aerodynamic roughness length over snow and ice surfaces. Using narrow physically plausible ranges of these parameters, we used an automatic multiobjective calibration technique (MOCOM-UA; Yapo et al., 1998) to find parameter sets that accurately reconstructed observed seasonal and annual mass accumulation and ablation on measured glaciers. As objective function elements, this multiobjective optimization used the root-mean-square error (RMSE) of winter (October–April), summer (May–September), and annual mass balance (aggregated over each glacier) and the absolute error in cumulative mass balance at the end of the calibration period. For glacier mass balance the entire period of record corresponding to the observations was used for calibration. This nontypical approach was used to prioritize the inclusion of more variability in the calibration period given the

short periods of observation (as few as seven years), over reserving a fraction of the observed period for validation alone.

After the optimal cryospheric parameter sets were found separately for each measured glacier in each basin, these parameters were then used for developing an initial spatially steady state field of glacier ice that will be used in historical glacio-hydrologic simulations. This initial field of glacier ice is obtained through spin-up simulations using the GDM off-line starting with ice free topography. To force the GDM, a spatially continuous field of annual mass balance was needed, and it is estimated by running the calibrated snow/ice melt model of DHSVM using the historical climate. The mean annual mass accumulation and ablation were calculated for every grid cell in each basin. Finally, this field of annual mass balance was used as a constant annual forcing for the GDM to spin-up glacier masses until a spatial steady-state of ice area and depth was obtained.

Considering the fact that many of glaciers in the region developed during colder/wetter climatic conditions, annual mass balance fields, used as input in the GDM, were perturbed locally by increasing annual mass balance as needed to match the spatial glacier cover developed from historical observations. In particular, such adjustments were required in areas with large glaciers that have longer response times to climate fluctuations. For instance, the South Cascade glacier in the North Cascade range, which, due to its thick ablation zone and shallow slope, exhibits a very strong negative mass balance and it is still adjusting to the end of the little ice age (LIA; Rasmussen and Conway, 2001). The spin-up procedure is detailed further in Frans et al. (2015) and Naz et al. (2014).

The earliest observation-based glacier extents that we aimed to reproduce in the glacier spin-up step were selected based on the availability of reliable historical spatial data. Depending on the basin these started early in the 20th century or 1950s and 1960s. The earlier period is close to the end of the LIA, and the midcentury period was characterized by a cold and wet period where many glaciers were stable or slightly advancing (e.g., Dick, 2013; Granshaw & Fountain, 2006). Given these two conditions, we targeted these periods for spin-up, avoiding periods where the glacier states would be highly transient.

Finally, using the glacier ice fields modeled in the glacier spin-up step as initial condition in the coupled DHSVM-GDM model and the calibrated snow/glacier accumulation and melt parameters, we focused on improving streamflow predictions at daily and seasonal timescales by adjusting several soil parameters that control subsurface flow, surface runoff generation, and storage of water in the soil column. These parameters are lateral transmissivity, porosity, maximum infiltration, and the *e*-folding depth used to decay transmissivity with depth. We used a simple model to estimate soil depths across the watershed as a function of local slope and upslope area derived from a 50-m DEM, by setting soil thickness limits to 0.15 and 2 m (Saulnier et al., 1997). This method produces thinner soils on steep slopes and ridges, and deeper soils in flat areas and depressions. Model performance was evaluated by comparing distributions of monthly streamflow volumes, the Nash Sutcliffe Efficiency (NSE) of flows at multiple temporal intervals, and daily flow duration curves with observations. We found manual calibration of spatially distributed soil parameters to be appropriate given that we did use optimization for snow/ice melt parameters, which have primarily influence on discharge patterns at coarse durations in these snowmelt dominated basins. Our analyses do not focus on short time intervals (e.g., daily) where soil parameters will have a stronger influence.

This calibration approach is unique as it incorporates a variety of observational data sources and follows a top down approach with respect to the simulation of mass in the watershed. Due to the variety of observational data sources and periods represented (e.g., discrete time slices of glacier area at decadal intervals and short periods of glacier mass measurements), the process did not follow traditional methods with well-defined calibration and validation periods. Where available, simulations are compared with observations for periods that were not included in calibration.

3.5. Describing Glacio-hydrological Change: 1960–2099

To identify regional patterns of glacio-hydrological response over the historical period and to infer how these patterns will evolve through the 21st century, model simulations encompassed the period 1960–2099, except the Nisqually and Hood River basins where simulations started in 1915 because the earliest glacier area estimates were available for that year for model initialization. Discharge comparisons used data from 1960 onward consistently for all of the basins. To characterize the future climate, we used an ensemble of 10 CMIP5 GCM output projections downscaled to the resolution of our historical forcing data (1/16°) using the

MACA methodology (Abatzoglou & Brown, 2012). We evaluated two emissions pathway scenarios: Representative Concentration Pathway (RCP) 4.5, a moderate warming scenario in which emissions stabilize by the end of the 21st century, and RCP8.5, a scenario in which emissions continue to increase through the 21st century. We developed an ensemble of predictions for each emissions scenario for each basin. To make comparisons between basins, the single historical time series and the mean of the ensemble of future predictions for glacier area and discharge were used as nondimensional variables by normalizing glacier area to the area for 1960 and summer streamflow to the historical mean for 1960–2010. Additionally, time series of these data are presented as 20-year center means to more clearly illustrate long-term fluctuations.

The relative contribution of glacier melt to streamflow was investigated in the summer months in the July–September period and in September, the month with least amount of basin wide snowmelt runoff and minimal rain. We define the glacier contribution to include the melting of glacier ice only (not including snow), as this represents loss from long-term storage rather than including the seasonal storage of snow on the glaciers.

To demonstrate the multiphased hydrologic response to glacier recession and its effect on trends in discharge, we analyzed how trends in discharge are manifested within the stream network and relate these to upstream glacier area. To demonstrate the effect of changes in glacier melt on trends in total streamflow, we calculated linear trends in total September discharge for each stream segment of a basin that shows a distinct peak in glacier melt in the middle of the 21st century. The trends were calculated for a period leading to the peak in glacier melt (2011–2050) and a period after the peak in glacier melt (2051–2099). We used Sen's slope estimator (Sen, 1968) to calculate trend magnitude and the Mann-Kendall statistic to test statistical significance (p-value < 0.05). The trend in each stream network reach is then compared against the fraction of upstream glacier cover at the beginning of the analysis period.

3.6. Cluster Classification of Glacier Areas

We use a statistical model to extrapolate the results of our simulations of glacier mass and area changes to glaciers across the PNW (United States). The river basins we modeled include 47% of the total area of glaciers and perennial snowfields (Fountain et al., 2017) in Oregon and Washington and encompass a representative range of physical settings. To extrapolate these results to the remainder of the glaciers in the region, we organized all of the glaciers in the region into classifications using a k-means clustering technique (Lloyd, 1982). We divided the full sample of PNW glaciers and perennial snowfields defined by Fountain et al. (2017) into three clusters based on mean winter and summer temperature and winter precipitation. We defined winter as months where the mean temperature is <0 °C (November–April) and summer as the months where the mean temperature is >0 °C (June–September). Climatological data were taken from PRISM normals corresponding to each glacier's centroid. These variables describe the climatic setting of each glacier. Elevation is implicitly represented through temperature. The longitudinal position in the maritime to continental climate transition and the effects of terrain shadowing of leeward slopes are represented through precipitation. Initially, we included more classes and other covariates in addition to precipitation and temperature in the cluster analysis (e.g., aspect and slope). We found that climate variables dominated cluster classification structure, particularly for the medium to large masses that are the largest contributors to basin runoff. Other covariates introduced unsystematic patterns into the classification of smaller glaciers that were difficult to find a physical explanation for. Granshaw and Fountain (2006) and Dick (2013) also found significant correlation between climate variables and glacier areas and no significant correlation for topographic variables (e.g., slope and aspect).

4. Results

4.1. Historical Reconstructions

We first reflect on the results of calibration and validation through historical reconstructions to build confidence in the conclusions drawn from model simulations. The parameter values found through the automatic calibration procedure reflect logical physical relationships (Table 3). For example, the strongest temperature lapse rates and highest snow albedo are in drier environments of the northern interior (Sandalee, North Klawatti, and South Cascade). While these temperature lapse rates reflect drier conditions, they are also stronger than observed values for the region (e.g., Minder et al., 2010). This likely indicates some compensation for unresolved warm biases attributed to the use of PRISM data in bias correction, which may introduce systematic errors in temperature measurements at high-elevation stations (Oyler et al., 2015). In contrast, weaker temperature lapse rates and lower snow albedo were found in more humid environments closer to the coast

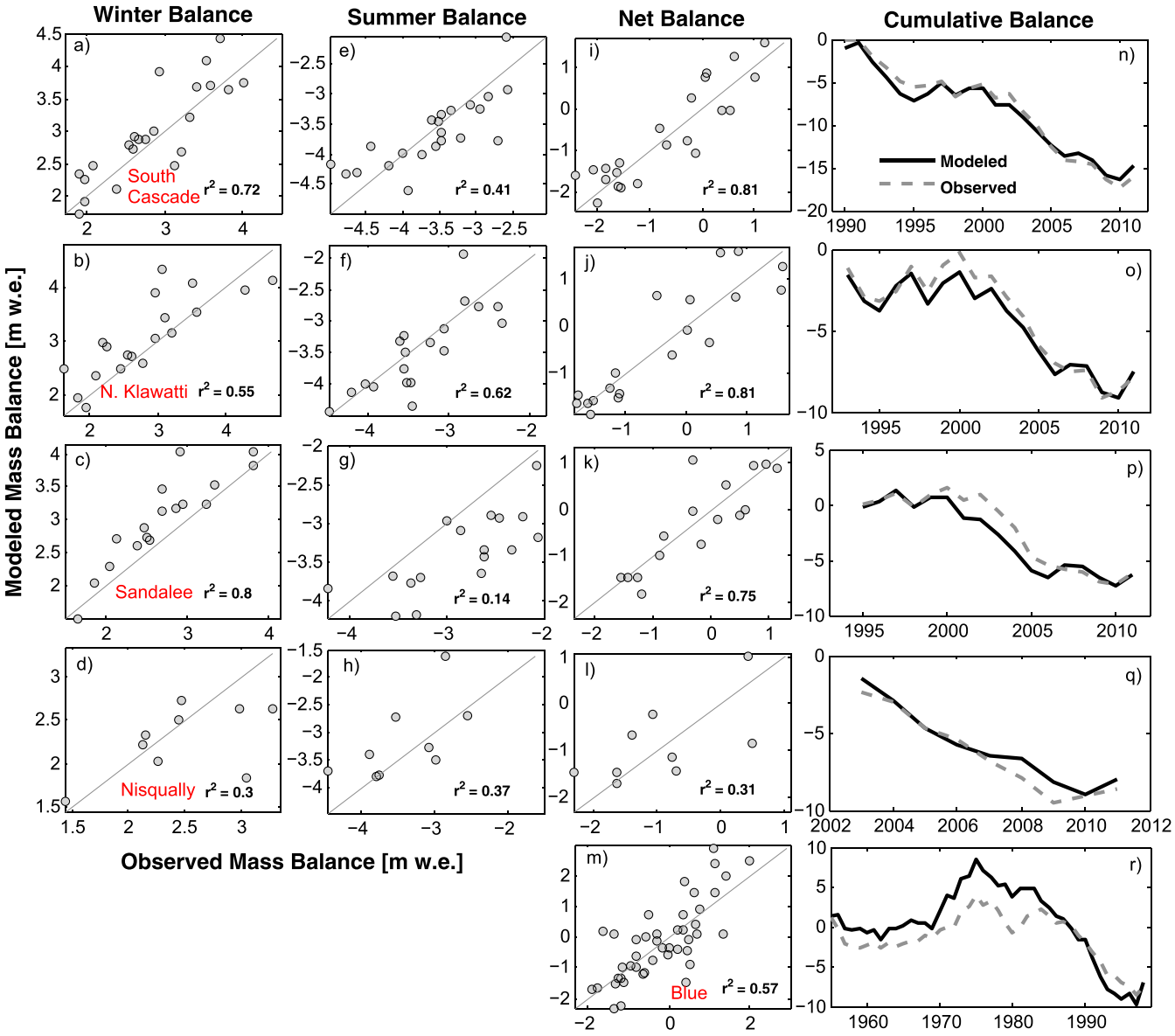

Figure 2. (a–m) Observed (*x* axis) and modeled (*y* axis) mass balance for the entire glacier. (n–f) Time series of observed and modeled cumulative mass balance for each glacier used in calibration. Only net annual mass balance observations were available for Blue glacier.

(Blue, Nisqually). Precipitation multipliers in excess of 1.0 were required for two glaciers, Sandalee Glacier (3.47) in the Stehekin watershed, and Blue Glacier (1.34) in the Hoh watershed. The precipitation of the 1/16° grid cell at the location of Sandalee Glacier was anomalously low as compared with all surrounding grid cells; hence, it represented an extreme local bias; this precipitation multiplier was only applied to the corresponding grid cell.

Comparisons of modeled and measured glacier mass balance (obtained from extrapolation of point measurements) vary in agreement (r^2 = 0.31–0.81; Figure 2). For the larger glaciers the comparison is reasonable (r^2 = 0.81, South Cascade and North Klawatti), but for the smallest glacier (r^2 = 0.75, Sandalee) and for the glacier with the shortest observation record (nine years) and the sparsest network of point measurements, the model performance was worse (Nisqually, r^2 = 0.31). For these two glaciers, nonclimatic processes such as wind redistribution of snow, glacier ice avalanching, and highly variable debris cover (both of which are not represented in the model) have a larger influence on net mass changes, which makes their mass balance more difficult to model and measure. The model is able to reproduce the general pattern of mass fluctuations

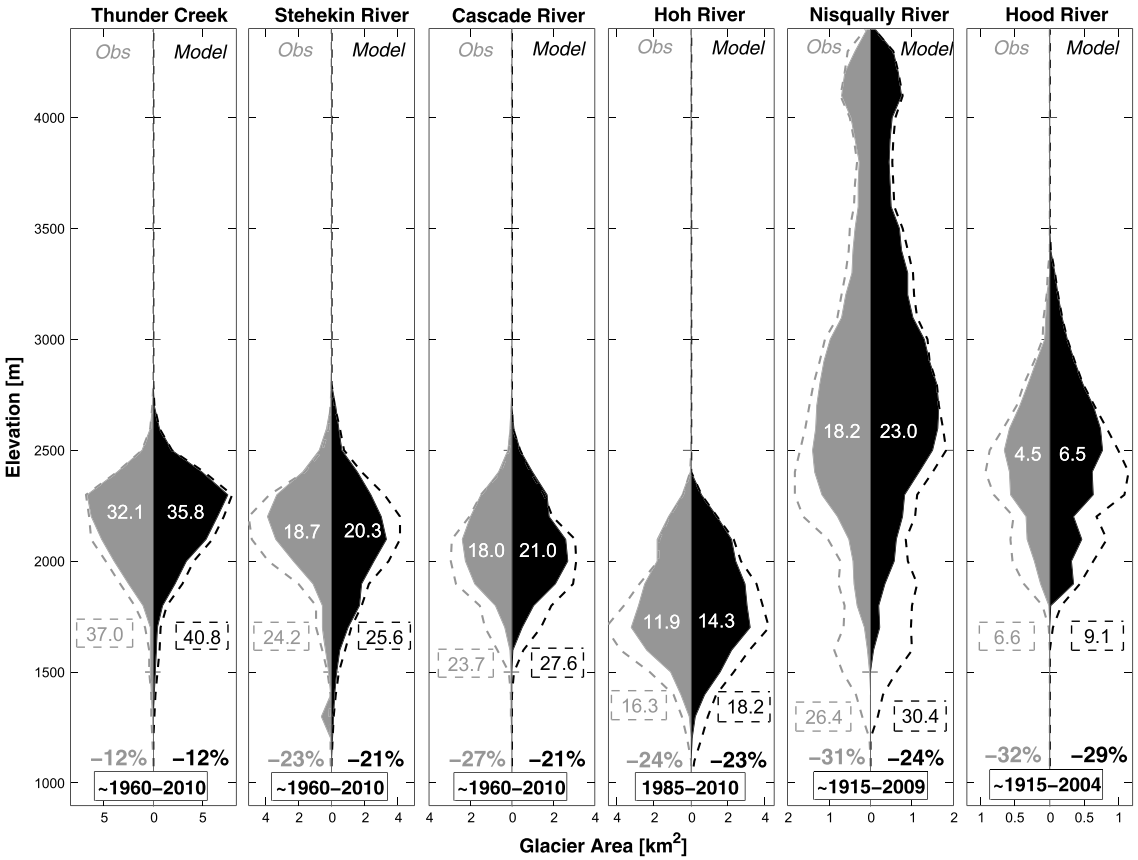

Figure 3. Observed and modeled distributions of glacier area according to elevation for historical (dashed) and recent (filled) periods of time. The period of analysis varies between basins and is reported at the bottom of each plot. For reference, the historical and recent total glacier area (km^2) is reported in the dashed boxes and filled areas, respectively. The relative change in glacier area is reported as a % over the period of analysis at the bottom of each plot. Note that the *x* axis (glacier area) intervals vary between basins.

of Blue Glacier (r^2 = 0.57); however, overestimation of mass accumulation occurred in the early 1970s. This is potentially linked to a bias in the precipitation forcing data during this period (see section 4.4 and Figure 6b).

The hypsometry of modeled and observed glacier area and its change over the historical time period was examined. For each of the six river basins we composited modeled and observed glacier area into 100-m elevation intervals for years corresponding to the earliest and most recent glacier area data available in each basin. Higher symmetry in the vertical plots indicates better model performance in predicting glacier area. The overall shapes of modeled and observed hypsometric distributions of glacier area compare well (Figure 3). The total glacier area is reported in the dashed boxes and filled areas for the historical and recent date, respectively. In general, glacier area is slightly overestimated as compared to observations. As compared with observationally derived boundaries, modeled valley glaciers typically are slightly wider due to the nature of the ice flow model and DEM resolution (Naz et al., 2014). Additionally, the model includes ice covered cells in small clusters that may be intermittent and not continuously connected to large ice bodies. These small features may not be captured in observationally derived area estimates.

The relative amount of modeled area change in each basin is in agreement with the observations. This provides support for the validation of the coupled simulation of glacier mass balance and dynamic ice flow. The largest loss of glacier area occurs in the Nisqually and Hood River basins; however, this is due to the longer period of analysis. The least recession is in Thunder Creek, the northernmost high-elevation basin. The lowest elevation basin, the Hoh River, shows a large recession over a relatively short period (1985–2010).

Finally, we illustrate model performance in predicting streamflow discharge in each basin for their period of calibration by comparing modeled and observed monthly mean streamflow (Figures 4f–4j) and daily

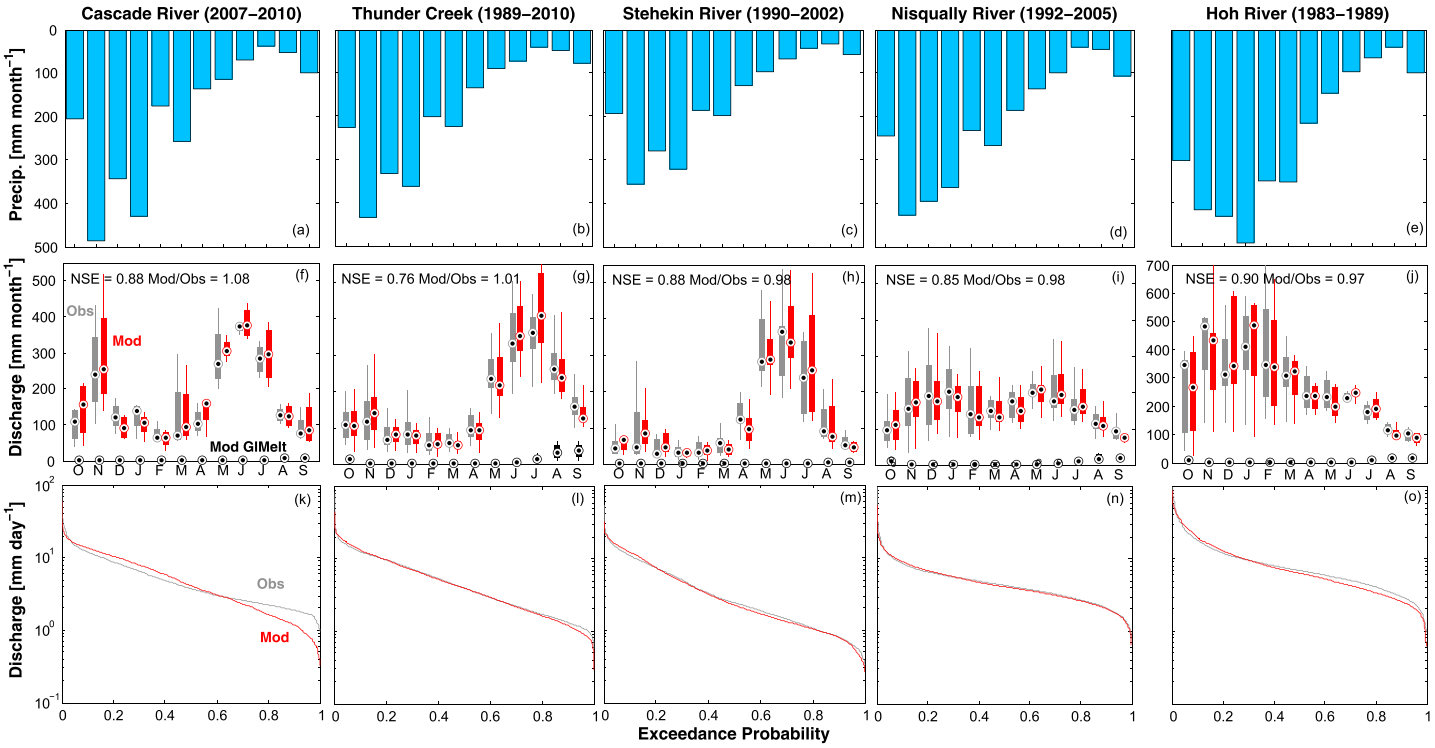

Figure 4. (a–e) Monthly mean precipitation, (f–j) modeled and observed monthly mean streamflow, and (k–o) modeled and observed exceedance probabilities of daily discharge for each river basin during the calibration periods. Red is used for modeled, and gray is used for observed data. Modeled glacier melt for the corresponding periods is shown in black for reference.

streamflow duration curves (Figures 4k–4o). The latter is plotted as exceedance probability, practically indicating that the fraction of year a given discharge is exceeded. For reference, mean monthly precipitation is also plotted (Figures 4a–4d) and model simulated glacier melt during the period of calibration (Figures 4f–4j). The seasonal timing of precipitation is ubiquitous, while the Hoh River receives the greatest amount and the Stehekin River the least. In general, the model captures seasonal discharge patterns and monthly variability well (monthly NSE = 0.76–0.9). Discharge is predicted consistent with observations in late summer (August–September) when glacier contribution to discharge is largest. The largest differences in modeled and observed flows were found in winter (December–January) low flows in the Cascade basin (Figures 4f and 4k). This is an artifact, a misrepresentation of the temperature regimes of individual warm winter extratropical storms, known as atmospheric rivers. The temperature profiles of these warm events are not captured well with the use of a constant temperature lapse rate. This underestimation of winter flow is commensurate with an overestimation of flow in early spring. To test the model's performance, we compared modeled and observed discharge during periods not included in the calibration. The calibration periods (displayed and listed in Figure 4) and validation periods varied basin to basin based on available observations. The model performance in the validation periods (monthly NSE = 0.78 for Cascade and ~0.85 for all other basins) was consistent with the performance during the period of calibration (Figures 4a–4e).

Table 4
Mean and Maximum Modeled Glacier Contribution to Summer (July–September) and Late Summer (September) Discharge Volumes for the Period 1960–2010

	July–September		September	
Basin	mean (Q_g/Q_{tot})	max (Q_g/Q_{tot})	mean (Q_g/Q_{tot})	max (Q_g/Q_{tot})
Cascade	0.05	0.13	0.15	0.54
Hoh	0.09	0.22	0.14	0.39
Nisqually	0.14	0.28	0.24	0.42
Stehekin	0.04	0.11	0.12	0.36
Thunder	0.12	0.27	0.28	0.63
Hood	0.02	0.07	0.06	0.11

4.2. Historical Role of Glacier Melt

On average the relative contribution of glacier melt to summer discharge is modest at the basin scale in most cases (2–14%), with the largest contribution of 14% in the Nisqually basin (Table 4). By September the relative contribution increases to 6–28%. The maximum contribution to September discharge over the time period is nearly double the mean

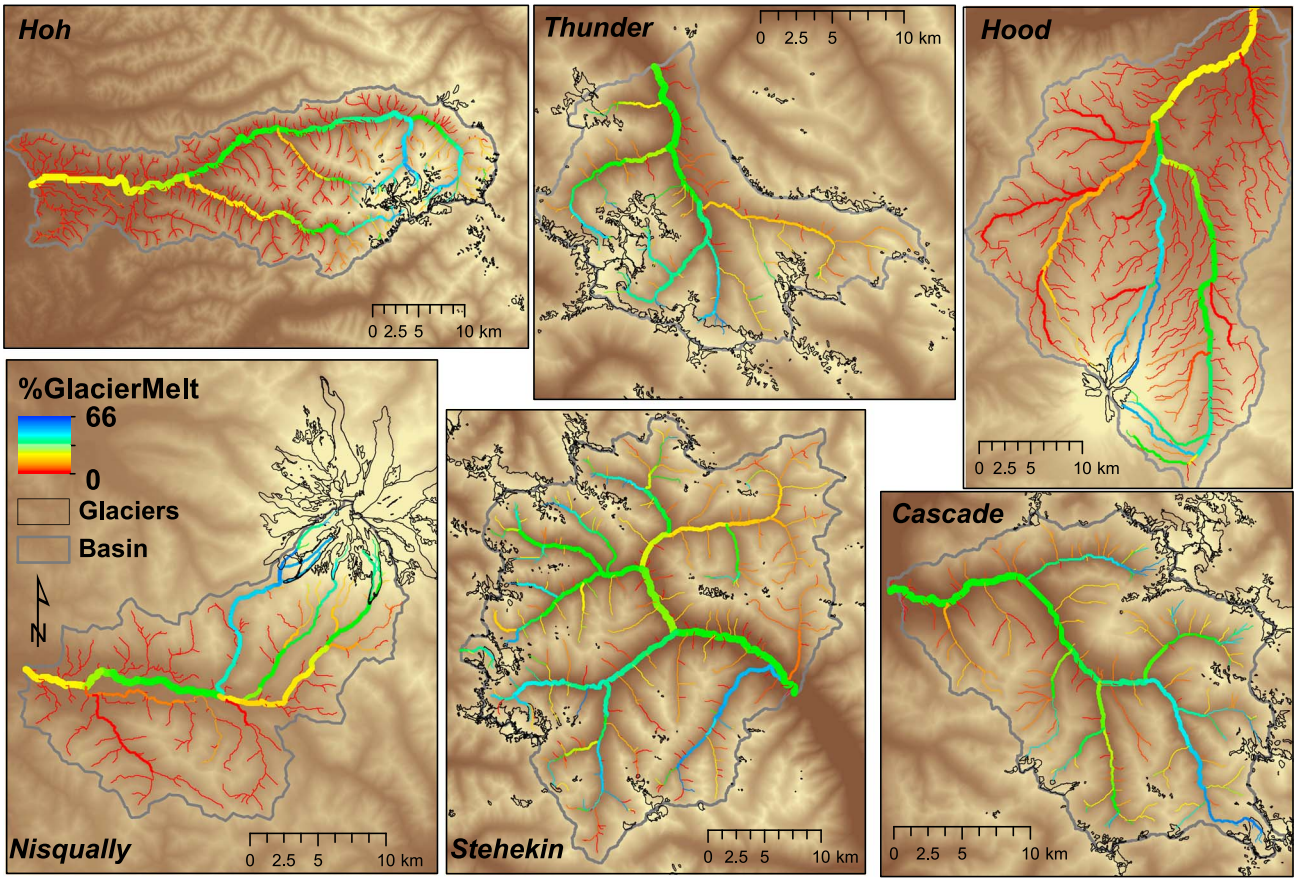

Figure 5. Mean percent glacier contribution to streamflow in September along the stream network of each study basin for the 1960–2010 period. The stream networks were defined based on local contributing area and routing of the digital elevation model surface and are used in the model for routing stream discharge. Network segment width is scaled by its discharge volume relative to discharge at the outlet.

value in most cases with a single-year maximum of 67% in the Thunder Creek basin. The years of maximum contribution occurred in the late 1980s to early 1990s and during water year 2005. Not surprisingly, the relative glacier contribution for each basin closely follows the relative glacier cover (Table 1).

The contribution of glacier melt at the outlets of the basins (defined by stream gauging locations) is typically small as shown in Table 4; however, the contribution is large in some upstream tributaries (Figure 5). The mean contribution of glacier melt to September discharge increases in upland stream segments in each river basin. In upstream locations the glacier contribution to September discharge is in the 50–66% range. This number may appear low for reaches almost entirely glacierized because our definition of the glacier contribution is limited to the melting of glacier ice only; seasonal snowmelt still contributes to runoff in high-elevation locations in September. There is also strong interannual variability in the glacier contribution. In years with cool temperatures and high precipitation the relative glacier contribution can be close to zero as the glaciers are covered with snow for most of the year; whereas in warm years the limited amount of seasonal snowmelt can result in relative glacier contributions as high as 90%.

4.3. Glacio-hydrological Change: 1960–2099

The annual temperature and precipitation relative to the means of 1960–2010 are shown in Figure 6. We smoothed the data using a 20-year centered moving average to more clearly show long-term trends. Under RCP8.5 air temperature is projected to increase steadily through the 21st century with the largest changes predicted for the interior basins (Cascade, Thunder, and Stehekin); up to 6 ^{o}C by the end of the century. The coastal Hoh River basin is projected to warm the least. In all of the basins, a general increasing trend in precipitation is observed in the smoothed ensemble means throughout the 21st century. This smoothed

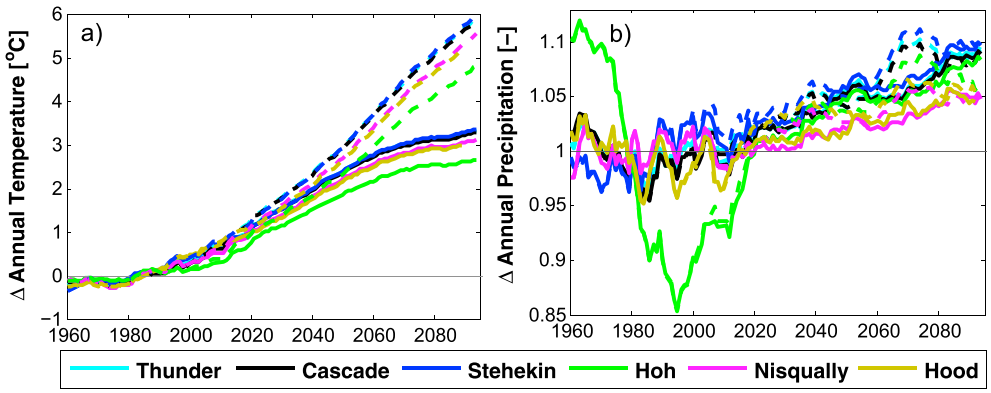

Figure 6. Historical and projected changes in basin average (a) annual temperature and (b) precipitation with respect to 1960–2010 means, presented as a 20-year centered moving average. Only the ensemble means of 10 downscaled global climate model outputs for each emission scenario are shown to demonstrate the central tendencies. Representative Concentration Pathway (RCP) 4.5 is represented with solid lines and RCP8.5 is shown with dashed lines.

ensemble mean of CMIP5 projections indicates increases of up to 10% of historical annual precipitation under both warming scenarios for all basins except the Nisqually and Hood River. An artificial strong drying trend over the historical period is apparent in the Hoh River data. Comparing this trend with biases manifested in the simulation of the mass balance of Blue glacier (section 4.1 and Figure 2r), we concluded that the Livneh et al. (2013) data contain some positive biases in precipitation for the Hoh basin during a short period in 1960s and early 1970s.

Historically, the modeled evolution of glacier area shows rapid losses, based on the longer period of Hood and Nisqually, until ~1950 (Figure 7). This is consistent with observations of glacier area reported in Jackson and Fountain (2007) for Mount Hood. This period was characterized by adjustments of glacier mass to the change of climate at the end of LIA and positive temperature anomalies in the 1930s (positive PDO index). At about midcentury, the climate shifted to a cooler and wetter regime with positive precipitation and negative temperature anomalies (negative PDO index), lending to stabilization and gains in modeled glacier mass and area in all basins until the early 1980s consistent with observations (Conway et al., 1999; Dick, 2013). The modeled and observed gains in area are most pronounced in the North Cascade range, as many of these glaciers are small and have faster response times to climate forcing (4–16 years; Pelto & Hedlund, 2001). Additionally, during this cold and wet period, relatively sharp increases and decreases in area are modeled. This is partially attributed to carry over seasonal snowpack densifying to ice, rather than advances of existing glaciers. Validating the model's ability to track ice formation beneath perennial snowpacks would be difficult; however, this is important to consider when comparing with observational glacier area data sets that may not capture these short-lived ice features.

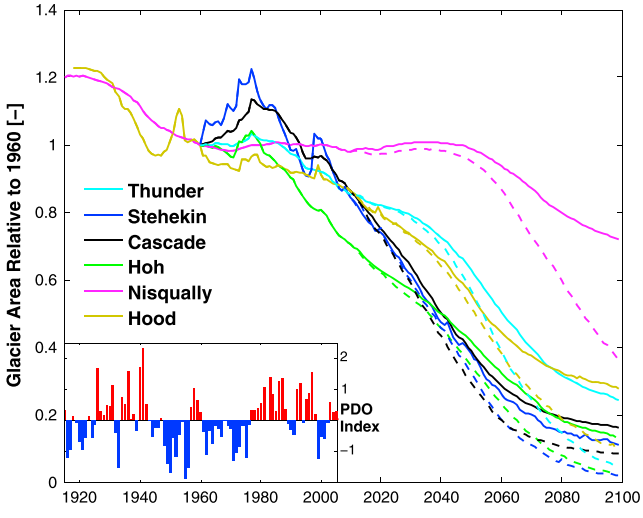

Figure 7. Modeled glacier area relative to the glacier area of 1960 for the modeled river basins. The solid lines represent the historical and ensemble mean of the Representative Concentration Pathway (RCP) 4.5 emission scenario, and the dashed lines represent the ensemble mean of RCP8.5. A time series of the Pacific Decadal Oscillation (PDO) index for the period 1915–2005 is provided on the inset.

After about 1980, glacier area declines are pervasive in all basins following a shift to warmer temperatures in a positive PDO phase superimposed on continued global warming. This historical response of glacier area to temperature is less than earlier in the century, which was marked by a transition from the climate at end of the LIA, evident in model results for the Nisqually and Hood basins and supported by broad observations in the region (e.g., Dick, 2013; Jackson & Fountain, 2007). The most rapid retreat is observed in the glaciers of the Hoh River basin located at the lowest elevations and in the warmer maritime climate region. The highest elevation basins (Nisqually, Thunder Creek, and Hood) display the slowest retreat until 2040 when the retreat increases rapidly. The smallest loss of glacier area is predicted for the Nisqually basin. These are the highest elevation glaciers we studied, located on southern flanks of Mt. Rainier (4,392 m). While these results reveal some distinct basin scale patterns of retreat

influenced by local hypsometry and climate, the general pattern of retreat is consistent with the regional model results of Clarke et al. (2015) for the glacierized regions north of our model domain in British Columbia for the period 1980–2100.

Extending the analysis into deeper detail than can be assessed with the ensemble mean reveals some interesting patterns for the high elevation basins. Some of the climate projections indicate periods of substantial increases in precipitation by the middle of the 21st century (Rupp et al., 2017). During this period, the relative amount of warming in these projections has less of an impact on precipitation phase at high elevations. Thus, increased precipitation can lead to slowing of mass loss, net annual gains in mass, and in the more extreme cases, temporary advancement of glaciers. For instance, small short-lived advances of glaciers are projected in some ensemble members in the Nisqually and Thunder creek basins, during the period of prior to 2040. The sensitivity and interplay between increased precipitation and warming temperatures can be observed in Thunder Creek projections of basin wide glacier volume, annual precipitation, and annual temperature (Figures 8a–8c). For reference a wet projection (RCP8.5 NorESM1-M) and one with high warming (RCP8.5 HadGEM2-CC) are highlighted in the ensemble. The wet projection shows increased precipitation early in the 20th century leading to substantial gains in basin wide glacier volume (Figure 8a). The warm projection has higher precipitation later in the century (~2070s; Figure 8b); however, there is no response in glacier mass to enhanced precipitation, as regional temperature continues to increase. The entire ensemble of meteorological forcing and glacio-hydrological simulations were used to examine the sensitivity of basin wide glacier mass to differences in precipitation and temperature (Figure 8d). In general, when projected annual precipitation is above the historical mean, and the annual mean temperature is <3 °C greater than the historical mean, basin wide gains in glacier mass are modeled more frequently. Above 3 °C the ability of increased precipitation to buffer mass losses from increases in temperature diminishes. For these glaciers an increase of 3 °C results in the mean winter temperature being greater than ~ -2 °C, a threshold above which snowpack sensitivity to precipitation strongly decays as greater amounts of snow fall as rain (e.g., Lute & Luce, 2017).

Next, we focused on the predicted consequences of changes in glacier mass on streamflow by examining the relative changes in snowmelt, rainfall, and glacier melt derived discharge. Continuous declines in total discharge from 1980 to 2099 are modeled in all of the basins (Figures 9a and 9e). The reduction in total discharge is highest in the Stehekin, Cascade, and Thunder basins. This is largely a result of continuous declines in nonglacial sources (snowmelt + rain; Figures 9b and 9f) in August and September. The primary change comes from impacts of warming on snowmelt and accumulation; historically, these basins have the strongest seasonal snowmelt signature (Figures 4f–4h). The largest decrease in total discharge predicted by the end of the 21st century is during August in these three basins under RCP8.5 (~80%).

A more complex pattern was observed in the modeled evolution of glacier melt (Figures 9c and 9g). Toward the end of the 1980s, modeled glacier melt began to decline in the Hoh, Stehekin, and Cascade River basins in both August and September. The rate of these declines are interrupted and lessened intermittently until 2000–2020, after which the rate of decline is consistently strong. Glacier melt in the Hood River basin is predicted to increase until early in the 21st century (~2000–2020) and decrease thereafter; however, its relative contribution is small at the basin scale (Figures 9d and 9h). In the basins that include the highest elevations with high initial glacier cover (Nisqually and Thunder), glacier melt decreases in the near future then continuously rises until peaking in the 2050s–2060s. The RCP8.5 emission scenario, with higher late century warming, amplifies these peaks. The reduction of glacier melt in Thunder and Nisqually basins (2000–2020) is another manifestation of increases in precipitation before significant warming occurs (Figures 6 and 8). The effect of these wetter periods in the historical and projected meteorological forcing leads to a reduction in snowline elevations, and increased extent and duration of snow cover on the glaciers, and culminated in a net reduction of modeled melt from the long term glacier ice storage for wet years in this period.

Changes in the relative contribution of glacier melt to streamflow do not always mimic the direction of changes in glacier melt itself (Figures 9d and 9h). Despite declines in glacier melt in the Hoh, Hood, Stehekin, and Cascade river basins the relative contribution of glacier melt increases until about midcentury during August, while it remains steady in September, due to more rapid declines in seasonal snowmelt. The relative contribution in August is also sustained longer due to the glaciers being exposed earlier in the year

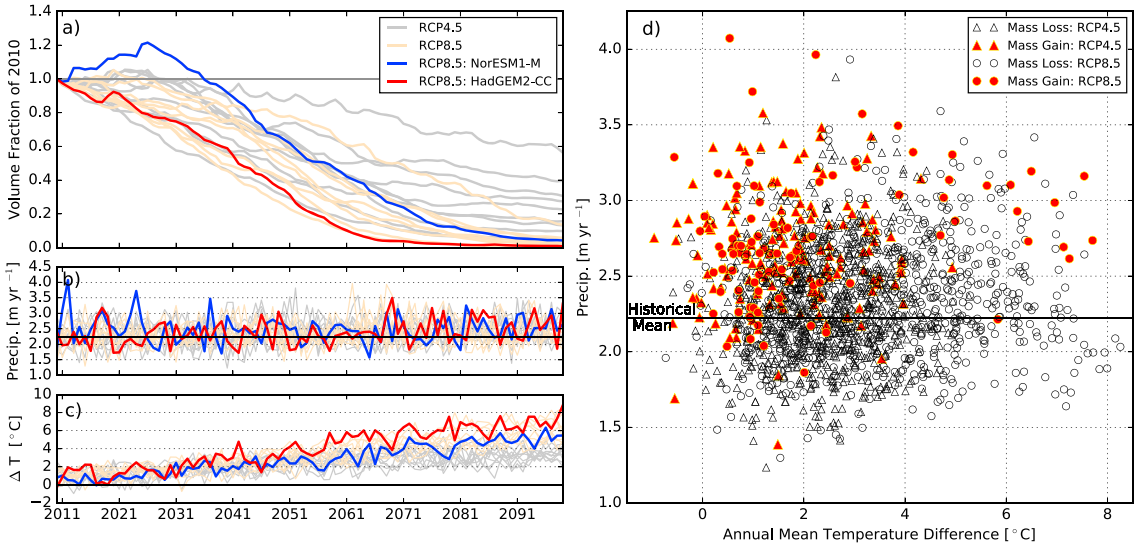

Figure 8. Thunder Creek: 20 model projections of (a) glacier volume normalized by the glacier volume of 2010, (b) annual precipitation of the model meteorological forcing data, (c) the difference between the annual mean temperature of the meteorological forcing data and the historical mean (1960–2010), and (d) annual precipitation versus mean annual temperature difference with respect to the historical mean (1960–2010) for all 20 projections. The red markers indicate a basin-wide gain in glacier volume for the given precipitation and temperature combination, where the black open markers indicate an annual loss of basin-wide glacier volume. (a–c) Two of the 20 projections are highlighted to more clearly illustrate glacier volume response to the projections with the wet (blue) and warm (red) climate forcing. Historical mean precipitation is presented as a horizontal line (b).

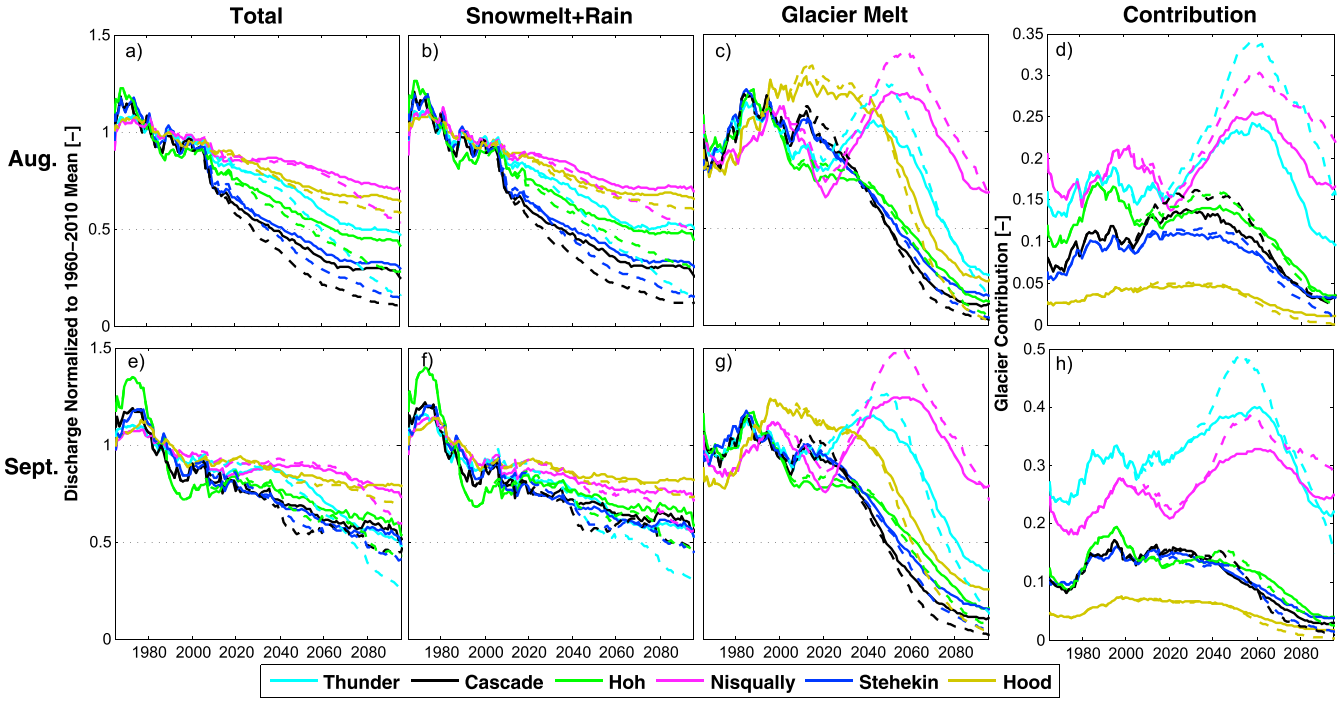

Figure 9. Twenty-year centered moving average of modeled hydrological fluxes for August (top row) and September (bottom row) normalized to their mean values for the 1960–2010: (a and e) total streamflow, (b and f) water input from of seasonal snowmelt and rain, (c and g) glacier melt, and (d and h) the relative contribution of glacier melt to streamflow. Simulations using Representative Concentration Pathway (RCP) 4.5 projections are shown with solid lines and RCP8.5 with dashed. For the historical period the lines represent a single simulation forced with observed meteorological data and the lines for the future period represent the means of an ensemble of projections forced with the downscaled output of 10 global climate models for each emission scenario.

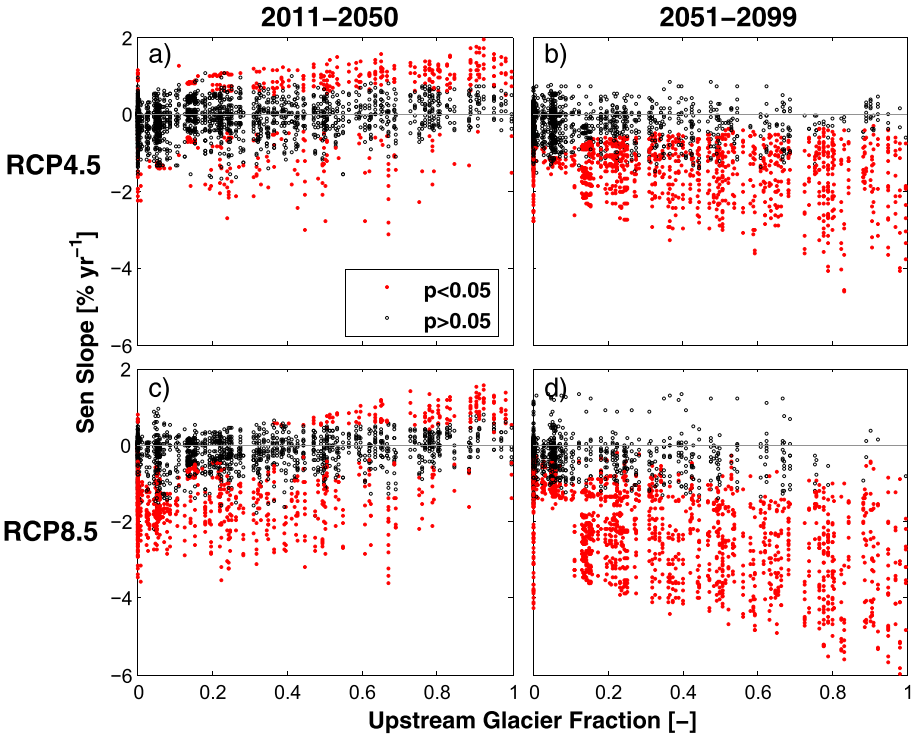

Figure 10. Linear trends in modeled September discharge volumes in each stream network segment in the Thunder Creek Basin for each of the 10 global climate model scenarios as a function of upstream glacier area. Trends were calculated using the Sen's slope estimator for the periods of (a and c) 2011–2050 and (b and d) 2051–2099. Trends with statistical significance (p-value < 0.05) are denoted with filled red circles and trends that are not statistically significant (p-value > 0.05) are shown with hollow black circles. Historical observed glacier area (~1960; Dick, 2013) was used to index upstream glacier area.

following shift of melting to earlier in the season. The primary reason for this is again tied to reduced snowpack, an earlier snowmelt season, and larger declines in snowmelt contribution to streamflow than glacier melt during the summer.

Among the basins we studied, Thunder Creek shows the highest variability in glacier melt contribution to streamflow with multiple peaks. Given the variable contribution of glacier melt to streamflow across the channel network, a natural question water managers could ask would be: how does the streamflow trend vary across the channel network in relation to upland glacier fraction? We examined the multiphased peak with increased granularity within the stream network of Thunder Creek following the trend analysis method outlined in section 3.5. This basin showed clear increases and decreases in glacier melt through the 21st century (Figures 9c and 9g). We compared modeled trends in discharge in each network segment to the upstream glacier area at the start of the historical period (Figure 10). In Figure 10, upslope watershed area decreases from left to right as the glacier fraction of the upstream watershed grows. Early in the 21st century negative trends in September total discharge are modeled in lower stream segments with low upstream glacier cover (up to ~ −4%/year) and positive trends are modeled in stream segments located closer to the glaciers with the highest upstream glacier cover (up to +2%/year; Figures 10a and 10c). During this period increasing discharge from highly glacierized areas offsets and buffers decreasing discharge from areas with low glacier cover as the amount of snowmelt declines over time. This can be observed in the modeled trajectory of total September discharge (Figure 9e). In the second half of the century after glacier melt peaked (Figure 9g) declining glacier melt drives negative trends in total discharge for stream segments in the low-order streams with high glacier cover (up to −6%/year; Figures 10b and 10d). This analysis provides an example of how changes in glacier melt discharge can both buffer and exacerbate negative trends from declining nonglacial sources (seasonal snowmelt) in high-elevation glacierized basins. This last point may provide further insight into patterns of low flow declines found in previous studies across the PNW. In these studies some of the declining trends reported in high-elevation partially glacierized areas are less severe and/or insignificant (e.g., Kormos

et al., 2016; Leppi et al., 2012). This modeling analysis provides a potential physical explanation for some of the incongruent patterns of historical declines in streamflow in the region.

4.4. Generalized Response of Glaciers and Glacier Melt in the PNW Region

We applied a k-means cluster classification method (section 3.6) to extrapolate the results of our modeling to other glacierized areas of the region. Several patterns emerge in the organization of cluster classifications (Figures 11a–11d and Table 5). The glaciers with the highest precipitation fall into class 1. These are located closest to the Pacific Ocean and also have the warmest winters (Western Olympic Range and Mount Baker). Class 2 includes glaciers located at low to moderate elevations in the eastern Olympic range and Western Cascade range. The glaciers with the least precipitation were classified as 3. These glaciers are mostly located on or east of the crest of the Cascade Range where a transition to a continental climate occurs, with the coldest winter temperatures and warmest summer temperatures (relative to other classes). Glaciers on the leeward slopes of the Olympic range also fall into this classification, as they are located in a dry region caused by terrain blocking of precipitation. Class 4 is composed of glaciers with moderate precipitation, and the coldest winter and summer temperatures indicating their high elevation. Class 4 includes glaciers on the region's stratovolcanoes, as well as high peaks in the interior North Cascade range.

For each glacier class, we aggregated the modeled glacier area and volume to compare and generalize the long-term response (Figures 11e–11l). Examining both area and volume changes illustrates the influence of modeled glacier dynamics on area response to climate fluctuations. Prior to 1980, classes 1 (maritime, high precipitation) and 4 (cold, high elevation) showed stable patterns of glacier area and volume, with some modest gains. For class 1 this response is defined mostly by the modeled maritime glaciers in the Olympic Range (Figure 11d). Stable conditions are consistent with observed patterns for the class 1 glaciers on Mount Baker in historical data (Harper, 1993; Dick, 2013), which were not modeled in the study. This provides some justification that the climatological classification scheme captures the nature of historical glacier response. Prior to 1980 modeled glaciers in class 2 (maritime, low precipitation) and 3 (continental, dry) lose volume, which does not translate to significant changes in area, indicating thinning. After 1980 all glacier classes begin losing volume, which resulted in losses in glacier area.

As one could expect, with a dry precipitation regime, the glaciers of class 3 show the strongest response to climate in both the historical and future time periods. In fact, the responses of each emission scenario are close in magnitude, indicating that even with smaller amounts of warming, these glaciers will lose mass and recede. This increased sensitivity can be linked to the dry precipitation regime of class 3 (Table 5). The next most sensitive class is class 1. This can be explained by warmer winter temperatures (Table 5) due to the lower elevations (e.g., Hoh River; Figure 3) as well as their proximity to the Pacific Ocean. Class 2 shows a narrow range of projections until the emission scenarios diverge later in the century. This class is dominated by glaciers small in size that lack accumulation areas large enough to gain significant amounts of mass during wet years. Additionally, this class is the least represented in the modeled domain (Figures 11a–11d). Class 4, the highest elevation glaciers, shows the least amount of reductions in glacier area and volume. Moreover, the projections for these glaciers exhibit some increases in area and volume linked to projected increased precipitation as was illustrated in section 4.4 for Thunder Creek (Figure 8).

The sensitivity of glacier mass to climate change in these generalized classes closely reflects theoretical temperature and precipitation based sensitivities of seasonal snowpack identified in previous studies. The historical mean winter temperature of classes 1 and 2 (Table 5) are near the threshold where April 1 snowpack shows less sensitivity to changes in precipitation, ~ −2 °C (Lute & Luce, 2017), at which above this threshold less precipitation falls as snow. Below this threshold, changes in precipitation have a stronger impact on snowpack in class 4, with the coldest temperatures and moderate precipitation, translating to potential gains in glacier mass from increased precipitation (section 4.3 and Figure 8). The sensitivity of class 3 is more directly related to precipitation as it has the smallest magnitude, lesser seasonal amplitude (e.g., Figure 4c), and shorter seasonal duration, as supported by analytical results of Woods (2009). These effects of seasonal precipitation characteristics on snowpack sensitivities translate to increased losses of ice mass through longer duration of exposure of the glacier ice.

The climatological classification of glaciers was extended to extrapolate predictions of peaks in glacier melt discharge across the region. For each of the 20 ensemble members used in this study, we plot the predicted

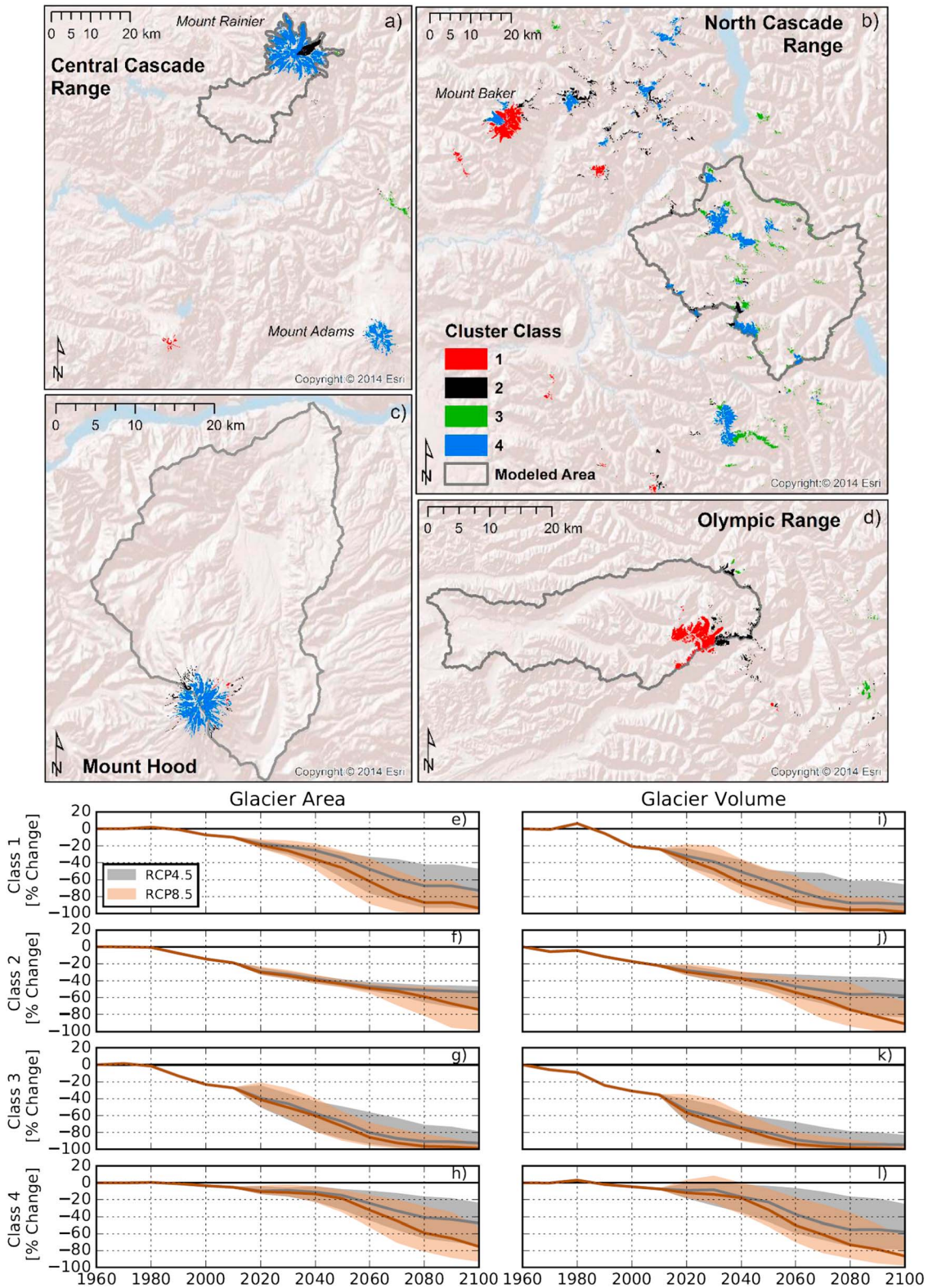

Figure 11. (a–d) Classification of PNW glaciers using K-means cluster analysis based on each glacier's local climatology defined by Parameter elevation Regression on Independent Slopes Model (PRISM). Glacier polygons were defined by Fountain et al. (2017). (e–h) Modeled historical and future projections of glacier area and (i–l) volume change for each aggregated cluster classification. The range is defined by the minimum and maximum amounts of projected losses in glacier area for the period 1960–2099 in modeled projections for the glaciers in the study basins. This range represents a 10-member ensemble of projections for each emission pathway scenario (Representative Concentration Pathway [RCP4.5] and RCP8.5). The historical simulation and the ensemble median is shown with the solid lines.

Table 5
Cluster Classification of Pacific Northwest U.S. Glaciers and Aggregated Historical Climatic Variables That Were Used to Assemble Each Classification

Cluster class	Winter temperature (°C)	Summer temperature (°C)	Winter precipitation (mm/yr)	Description
1	−2.8	8.9	3652	Maritime: high precip, low elevation, warm winter
2	−2.5	9.7	2220	Maritime: low-mid elevation, leeward Olympics, W. Cascades
3	−4.8	8.4	1561	Dry: continental transition east of cascade crest, Olympic rain shadow
4	−5.8	6.9	2447	High Elevation: cold winters and summers, moderate precip.

peak in the 20-year centered moving average of glacier melt discharge for each basin (Figure 12a). Uncertainty in the timing of the peak in glacier melt is represented in the spread between projections for each emission scenario. The peak in glacier melt varies between basins (section 4.4 and Figure 9). In general, glacier melt in the higher elevation basins (Thunder and Nisqually) was modeled to peak later in the century and the peaks occurred in the historical period in basins with low elevation glaciers (Hoh and Cascade) or glaciers with low precipitation (Stehekin). Projections using the two different emission scenarios do not suggest significant differences in the timing of peaks in the study river basins; although in the two high elevation basins, Nisqually and Thunder Creek, more warming (RCP 8.5) tend to cause later peaks as evidenced by the median values. In many individual projections there can be multiple peaks attributed to natural variability within the observation/GCM meteorological data, superimposed over a long-term trend. This can increase the spread of predictions of peak glacier melt discharge, particularly for the emissions scenario with lesser warming (RCP4.5, e.g., Thunder).

We related these predictions of peak response of each basin to the dominant glacier class in each glacierized watershed in the region to facilitate a regional understanding of the timing glacier melt discharge response. The relative fraction of each glacier classification in the modeled basins is reported under the basin name (Figure 12a). Each watershed in the region was defined by the 10 digit hydrological unit code classification (HUC10) of the National Hydrographic Dataset (USGS, https://nhd.usgs.gov/). Each of these watersheds was assigned a glacier class based on the dominant class present (Figure 12b). Relating the model predictions of peak response to the watershed scale glacier classifications we inferred that (1) glacier melt in many of the watersheds in the eastern Cascade Range (class 3, 34% of glacierized watersheds by area) and low-

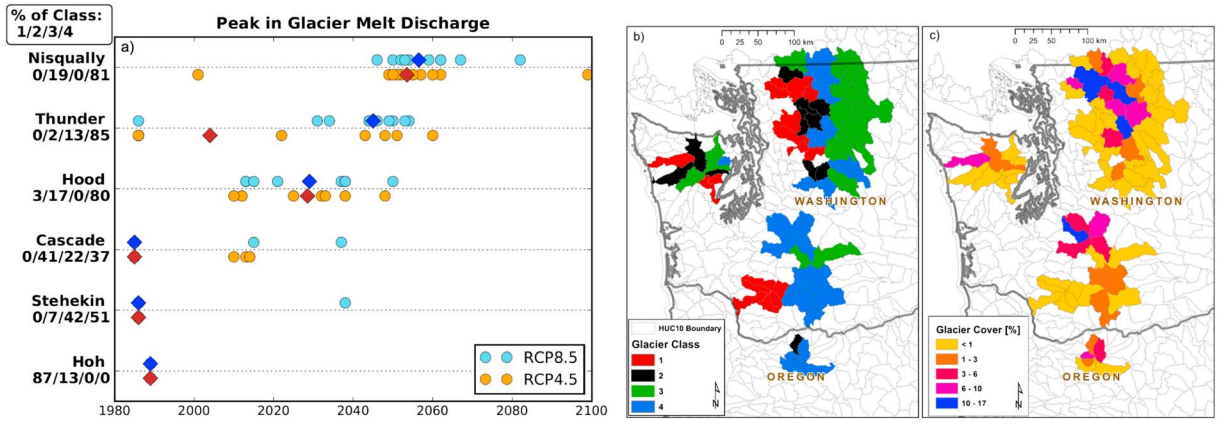

Figure 12. (a) Modeled peak in 20-year mean glacier melt discharge for each of the 20 ensemble members for each basin. The median of peak projections for each basin and emission scenarios are denoted with diamonds. The relative percentage of each glacier class in each basin is listed below each basin's label. (b) Ten-digit Hydrological Unit Code boundaries (HUC10) for the study region. HUC10 watersheds that contain glaciers are shaded with a color, which denotes the dominant glacier class in the watershed. (c) The relative glacier cover of each of the HUC10 glacierized watersheds.

moderate elevation maritime watersheds in the western cascades and Olympics (classes 1–2, 19%, 12% of glacierized watersheds by area) have already peaked or will peak in the current decade. The extrapolation of the predictions of peak response for watersheds that are dominated by class 4 glaciers (35% of glacierized watersheds by area) is more challenging, as these reflect a larger range of uncertainty (Figure 12a) with peaks of individual projections ranging from the 1990s to ~2100 in the most extreme cases. However, the most agreement in the prediction of peak response in these watersheds is in the 2030–2060 period. This qualitative extrapolation infers the timing of peak glacier melt response but does not indicate the relative contribution of glacier melt to total discharge of these watersheds. The relative glacier cover in many of these watersheds is small (Figure 12c); 61% of the glacierized watersheds have glacier cover of less than 1%. However, even with low glacier cover (Table 1), glacier melt contribution can be significant (Table 4; e.g., Huss & Hock, 2018). Due to uncertainties in the ranges of projected peaks, and the simple method of classification, this extrapolation remains a qualitative extension of the physically based modeling results; nevertheless, it is informative of potential regional spatial patterns of the peak response of glacier melt.

5. Discussion

The k-means cluster analysis provided a method for the spatial extrapolation of results of detailed modeling to the remaining glaciers of the region. The classification considered climatological aspects, as sensitivity of these is most robustly captured by our modeling on larger glacier surfaces. There are numerous small glaciers that are influenced by more nuanced local mass balance processes (e.g., local shading, avalanching, and wind redistribution), which would likely deviate from these climatological based classification projections. Small glaciers have highly variable sensitivities to temperature increases (Huss & Fischer, 2016) for which more detailed fine-scale modeling would be preferred over statistical extrapolation.

The results presented above reveal uncertainty with respect to future climate (ensemble of GCMs and two emission scenarios) but lack treatment of uncertainty stemming from other elements of the modeling chain including the initial state of ice, hydrological model parameters, and climate downscaling. Previous applications of the DHSVM-GDM glacio-hydrological model have explored parameter sensitivities and the implications for long-term projections. Naz et al. (2014) identified the relative influence of differing bed topography estimates, on the initial ice estimates to be relatively minor, with a maximum difference of ~10% of ice volume. Additionally, Naz et al. evaluated multiple sets of calibrated soil parameters of equal Pareto optimality and found there to be minor differences in the modeled summer streamflow patterns and the resulting quantification of glacier melt contribution for a historical period. Frans et al. (2015) provided a sensitivity analysis of the snow/ice melt, climate distribution, and ice flow parameters and the implications for long-term glacier and discharge projections. These parameters can have significant impact on resulting projections of discharge and glacier area, particularly when they are not selected based on performance of historical reconstructions. The supporting information of Clarke et al. (2015) provide detailed sensitivity analyses of parameters and assumptions of the GDM. To maintain conciseness, we did not repeat these sensitivity and uncertainty analyses of previous model applications for this study. Consequently, some methodological elements of our projections were applied in a manner such that uncertainty may be under represented through the modeling process (e.g., Clark et al., 2016).

Another source of considerable uncertainty for projections of glaciers is linked to projections of orographic precipitation. Coarse resolution GCMs are downscaled to better reflect the effect of finer resolution features, namely, the topography. This study used projections produced from a statistical downscaling product (MACA), which inherits projected changes in precipitation from GCM output, however imposes stationarity in the orographic influences precipitation. An alternative approach would be to employ dynamical downscaling, using a regional climate model that simulates circulation patterns resulting from the large-scale projections of climate change and interactions with finer-scale regional topography and water bodies. Several such studies have found different orographic precipitation patterns than were observed historically, locally amplifying, or decreasing the change in precipitation projected in the GCM forcing (Ashfaq et al., 2016; Salathé et al., 2010; Salathé Jr et al., 2008). Furthermore, Luce et al. (2013) hypothesize that weakened lower-tropospheric flow in the region projected by GCMs has the potential to decrease the orographic enhancement of precipitation. This may have a considerable impact on projections of the mass of higher elevation glaciers given the sensitivity of glacier mass fluctuations to precipitation changes coupled with modest

amounts of warming (section 4.3 and Figure 8). Model forcing uncertainties due to different downscaling methods should be studied in this region for improved prediction of future glacier masses and water resources.

Separating rain, snow, and glacier ice components of discharge is challenging (Weiler et al., 2018). While glacier melt is calculated at each grid cell of the model, DHSVM mixes rainfall and meltwaters from glacier ice and snow within the soil column or over bedrock as it routes flow on the landscape. As a result, individual sources of water cannot be explicitly tracked in streams. To calculate the relative volume of glacier melt in streamflow hydrographs, paired simulations with and without the representation of glacier masses were compared. This approach centers on the mass introduced by glacier melt as the primary difference in simulations, however neglects the influence of the presence of glaciers on evaporation from the soil surface and the routing of snowmelt and rain through glacier ice, which was neglected in the model for simplicity. Details on model assumptions are given in Naz et al. (2014) and Frans et al. (2015). A comparison of model derived glacier contribution with the contribution estimated from geochemical sampling is provided in Frans et al. (2016).

A common theme in glacio-hydrological literature is describing and predicting the occurrence of *peak water* (e.g., Baraer et al., 2012; Immerzeel et al., 2013). Recently, Huss and Hock (2018) approached this question for large river basins across the globe. The study included several basins in the PNW for which to draw comparisons with our findings and methodologies. In western North America Huss and Hock find peak water to have passed or approaching in the coming decade. This is consistent with the results of the warmer maritime and drier watersheds we modeled; however, we illustrate more complex patterns at higher elevations where glacier melt continues to increase well into the 21st century. As noted by Huss and Hock and this study, peak water timing can vary within a river basin and some of these details may be absent with larger applications, however are important for regional water and resource management. In higher elevations, we found a large range in predictions for peak water timing for the lower emissions scenario (Figure 12a), consistent with ranges of predictions of peak water in other regions (e.g., Clarke et al., 2015). This is attributed to sensitivities to precipitation and its variability in projections between GCMs. Moreover, this highlights potential risks of using small numbers of climate projections and relying on the single predictions represented by means of ensembles.

6. Conclusions

Glacierized watersheds of the PNW are among a global population facing significant glacio-hydrological change in the 21st century. This study describes complex interconnected hydrological and glaciological processes within temperate glacierized watersheds and illustrates their sensitivities to climate variability and change. Furthermore, this work represents the first application of physically complex high resolution modeling to generalize the glacio-hydrological patterns of the region, both historically and under future climate change. Our findings indicate the following:

- Long-term negative trends in glacier area are pervasive throughout the region; however, historical and projected climate variability, largely precipitation, can influence short-term deviations and offsets from the long term pattern. The relative influence of increased precipitation diminishes with warming temperatures. Above ~3 °C of warming, increased precipitation will have a diminished ability to partially offset glacier losses from increased melt in high-elevation basins.
- The glacier volume of two regions of the PNW shows the greatest sensitivities to warming temperature, however demonstrate distinctly different mechanisms for these sensitivities: (1) maritime low-moderate elevation glaciers with warm winters and (2) drier watersheds located east of the crest of the Cascade Range.
- Glacier melt in river basins at high elevations is expected to peak mid-to-late 21st century where the peak in glacier melt from other basins has already passed.
- Regardless of the trend direction in glacier melt discharge, its relative contribution to late summer streamflow is amplified due to the effects of declining seasonal snowmelt. This amplified contribution of glacier melt and its capacity to buffer low flows declines around 2020–2040 for all subregions except the high-elevation watersheds, where the increase in contribution can extend until late in the century.
- In glacierized river basins experiencing more rapid retreat, declines in glacier melt can further exacerbate negative trends in summer streamflow driven by reductions in seasonal snowmelt leading up to 80% reduction in late summer discharge volumes by the end of the century.

Detailed modeling and observational studies of glacio-hydrological processes can continue to be assimilated for regional scale monitoring and projections of glacio-hydrological change. As computational resource constraints are reduced with advances in high-performance computing technologies there will be less of a need to rely on extrapolation techniques and coarse scale modeling for similar regional analyses. Also, remote sensing observation and processing techniques to monitor glacier mass changes have advanced substantially in recent years (e.g., Rabatel et al., 2016; Shean et al., 2016). This will provide more observational data sets to define past and current glacier mass response to develop and constrain new modeling techniques for predicting future change.

Acknowledgments
We thank two anonymous reviewers, Erin Whorton and Editor Charles Luce, for their thoughtful suggestions and comments. These greatly improved the manuscript. Glacio-hydrological model data presented in this manuscript are available at: http://doi.org/10.5281/zenodo.1407650. Sources of data for model input and testing are listed in Table 2. This research was supported by NASA Interdisciplinary Research in Earth Science Program (grant number NNX10AP90G), Seattle City Light, and NSF PREEVENTS program (ICER 1663859). Fountain's participation was supported by US Geological Survey grant, G16AC00114.

References

Abatzoglou, J. T., & Brown, T. J. (2012). A comparison of statistical downscaling methods suited for wildfire applications. *International Journal of Climatology*, *32*(5), 772–780. https://doi.org/10.1002/joc.2312

Ashfaq, M., Rastogi, D., Mei, R., Kao, S. C., Gangrade, S., Naz, B. S., & Touma, D. (2016). High-resolution ensemble projections of near-term regional climate over the continental United States. *Journal of Geophysical Research-Atmospheres*, *121*, 9943–9963. https://doi.org/10.1002/2016JD025285

Baraer, M., Mark, B. G., McKenzie, J. M., Condom, T., Bury, J., Huh, K., et al. (2012). Glacier recession and water resources in Peru's Cordillera Blanca. *Journal of Glaciology*, *58*(207), 134–150.

Bernhardt, M., & Schulz, K. (2010). SnowSlide: A simple routine for calculating gravitational snow transport. *Geophysical Research Letters*, *37*, L11502. https://doi.org/10.1029/2010GL043086

Bohn, T. J., Livneh, B., Oyler, J. W., Running, S. W., Nijssen, B., & Lettenmaier, D. P. (2013). Global evaluation of MTCLIM and related algorithms for forcing of ecological and hydrological models. *Agricultural and Forest Meteorology*, *176*, 38–49. https://doi.org/10.1016/j.agrformet.2013.03.003

Burns, P., & Nolin, A. (2014). Using atmospherically-corrected Landsat imagery to measure glacier area change in the Cordillera Blanca, Peru from 1987 to 2010. *Remote Sensing of Environment*, *140*, 165–178. https://doi.org/10.1016/j.rse.2013.08.026

Clark, M. P., Wilby, R. L., Gutmann, E. D., Vano, J. A., Gangopadhyay, S., Wood, A. W., et al. (2016). Characterizing uncertainty of the hydrologic impacts of climate change. *Current Climate Change Reports*, *2*(2), 55–64. https://doi.org/10.1007/s40641-016-0034-x

Clarke, G. K., Jarosch, A. H., Anslow, F. S., Radić, V., & Menounos, B. (2015). Projected deglaciation of western Canada in the twenty-first century. *Nature Geoscience*, *8*(5), 372–377. https://doi.org/10.1038/ngeo2407

Conway, H., Rasmussen, L. A., & Marshall, H. P. (1999). Annual mass balance of Blue Glacier, USA: 1955–97. *Geografiska Annaler. Series A, Physical Geography*, *81*(4), 509–520. https://doi.org/10.1111/j.0435-3676.1999.00080.x

Cristea, N. C., Lundquist, J. D., Loheide, S. P., Lowry, C. S., & Moore, C. E. (2014). Modelling how vegetation cover affects climate change impacts on streamflow timing and magnitude in the snowmelt-dominated upper Tuolumne Basin, Sierra Nevada. *Hydrological Processes*, *28*(12), 3896–3918. https://doi.org/10.1002/hyp.9909

Cuffey, K. M., & Paterson, W. S. B. (2010). *The physics of glaciers*. Amsterdam: Elsevier Science.

Cuo, L., Beyene, T. K., Voisin, N., Su, F., Lettenmaier, D. P., Alberti, M., & Richey, J. E. (2011). Effects of mid-twenty-first century climate and land cover change on the hydrology of the Puget Sound basin, Washington. *Hydrological Processes*, *25*(11), 1729–1753. https://doi.org/10.1002/hyp.7932

Daly, C., Neilson, P., & Phillips, D. L. (1994). A statistical-topographic model for mapping climatological precipitation over mountainous terrain. *Journal of Applied Meteorology*, *33*(2), 140–158. https://doi.org/10.1175/1520-0450(1994)033<0140:ASTMFM>2.0.CO;2

DeVisser, M. H., & Fountain, A. G. (2015). A century of glacier change in the Wind River Range, WY. *Geomorphology*, *232*, 103–116. https://doi.org/10.1016/j.geomorph.2014.10.017

Dick, K. A. (2013). Glacier change in the north cascades, Washington: 1900–2009. Dissertations and Theses. Paper 1062. doi:https://doi.org/10.15760/etd.1062

Elsner, M. M., Cuo, L., Voisin, N., Deems, J. S., Hamlet, A. F., Vano, J. A., et al. (2010). Implications of 21st century climate change for the hydrology of Washington State. *Climatic Change*, *102*(1–2), 225–260. https://doi.org/10.1007/s10584-010-9855-0

Fernández, A., & Mark, B. G. (2016). Modeling modern glacier response to climate changes along the Andes Cordillera: A multiscale review. *Journal of Advances in Modeling Earth Systems*, *8*(1), 467–495. https://doi.org/10.1002/2015MS000482

Finger, D., Heinrich, G., Gobiet, A., & Bauder, A. (2012). Projections of future water resources and their uncertainty in a glacierized catchment in the Swiss Alps and the subsequent effects on hydropower production during the 21st century. *Water Resources Research*, *48*, W02521. https://doi.org/10.1029/2011WR010733

Fountain, A. G., Glenn, B., & Basagic, H. J. IV (2017). The geography of glaciers and perennial snowfields in the American West. *Arctic, Antarctic, and Alpine Research*, *49*(3), 391–410. https://doi.org/10.1657/AAAR0017-003

Frans, C., Istanbulluoglu, E., Lettenmaier, D. P., Clarke, G., Bohn, T. J., & Stumbaugh, M. (2016). Implications of decadal to century scale glacio-hydrological change for water resources of the Hood River basin, OR, USA. *Hydrological Processes*, *30*(23), 4314–4329.

Frans, C., Istanbulluoglu, E., Lettenmaier, D. P., Naz, B. S., Clarke, G. K., Condom, T., et al. (2015). Predicting glacio-hydrologic change in the headwaters of the Zongo River, Cordillera Real, Bolivia. *Water Resources Research*, *51*, 9029–9052. https://doi.org/10.1002/2014WR016728

Freudiger, D., Kohn, I., Seibert, J., Stahl, K., & Weiler, M. (2017). Snow redistribution for the hydrological modeling of alpine catchments. *WIREs Water*, *4*. n/a, e1232. doi:https://doi.org/10.1002/wat2.1232

Granshaw, F. D., & Fountain, A. G. (2006). Glacier change (1958–1998) in the north Cascades national park complex, Washington, USA. *Journal of Glaciology*, *52*(177), 251–256. https://doi.org/10.3189/172756506781828782

Harper, J. T. (1993). Glacier terminus fluctuations on Mount Baker, Washington, USA, 1940–1990, and climatic variations. *Arctic and Alpine Research*, *25*(4), 332–340.

Huss, M., & Fischer, M. (2016). Sensitivity of very small glaciers in the Swiss Alps to future climate change. *Frontiers in Earth Science*, *4*, 34.

Huss, M., & Hock, R. (2018). Global-scale hydrological response to future glacier mass loss. *Nature Climate Change*, *8*(2), 135–140.

Immerzeel, W. W., Pellicciotti, F., & Bierkens, M. F. P. (2013). Rising river flows throughout the twenty-first century in two Himalayan glacierized watersheds. *Nature Geoscience*, *6*(9), 742–745. https://doi.org/10.1038/ngeo1896

Jackson, K. M., & Fountain, A. G. (2007). Spatial and morphological change on Eliot Glacier, Mount Hood, Oregon, USA. *Annals of Glaciology*, *46*(1), 222–226. https://doi.org/10.3189/172756407782871152

Jansson, P., Hock, R., & Schneider, T. (2003). The concept of glacier storage: A review. *Journal of Hydrology*, *282*(1–4), 116–129. https://doi.org/10.1016/S0022-1694(03)00258-0

Jarosch, A. H., Schoof, C. G., & Anslow, F. S. (2013). Restoring mass conservation to shallow ice flow models over complex terrain. *The Cryosphere*, *7*(1), 229–240. https://doi.org/10.5194/tc-7-229-2013

Jost, G., Moore, R. D., Menounos, B., & Wheate, R. (2012). Quantifying the contribution of glacier runoff to streamflow in the upper Columbia River Basin, Canada. *Hydrology and Earth System Sciences*, *16*(3), 849–860. https://doi.org/10.5194/hess-16-849-2012

Jost, G., Moore, R. D., Weiler, M., Gluns, D. R., & Alila, Y. (2009). Use of distributed snow measurements to test and improve a snowmelt model for predicting the effect of forest clear-cutting. *Journal of Hydrology*, *376*(1-2), 94–106. https://doi.org/10.1016/j.jhydrol.2009.07.017

Kormos, P., Luce, C., Wenger, S. J., & Berghuijs, W. R. (2016). Trends and sensitivities of low streamflow extremes to discharge timing and magnitude in Pacific Northwest mountain streams. *Water Resources Research*, *52*, 4990–5007. https://doi.org/10.1002/2015WR018125

Laramie, R. L., & Schaake, J. D. (1972). *Simulation of the continuous snowmelt process. Ralph M. Parsons Laboratory for Water Resources and Hydrodynamics*. Cambridge, Massachusetts: Massachusetts Institute of Technology.

Leppi, J. C., DeLuca, T. H., Harrar, S. W., & Running, S. W. (2012). Impacts of climate change on August stream discharge in the Central-Rocky Mountains. *Climatic Change*, *112*(3–4), 997–1014. https://doi.org/10.1007/s10584-011-0235-1

Livneh, B., Rosenberg, A., Lin, C., Nijssen, B., Mishra, V., Andreadis, K. M., et al. (2013). A long-term hydrologically based dataset of land surface fluxes and states for the conterminous United States: Update and extensions. *Journal of Climate*, *26*(23), 9384–9392. https://doi.org/10.1175/JCLI-D-12-00508.1

Lloyd, S. (1982). Least squares quantization in PCM. *IEEE Transactions on Information Theory*, *28*(2), 129–137. https://doi.org/10.1109/TIT.1982.1056489

Luce, C. H., Abatzoglou, J. T., & Holden, Z. A. (2013). The missing mountain water: Slower westerlies decrease orographic enhancement in the Pacific Northwest USA. *Science*, *342*(6164), 1360–1364.

Lute, A. C., & Luce, C. H. (2017). Are model transferability and complexity antithetical? Insights from validation of a variable-complexity snow model in space and time. *Water Resources Research*, *53*, 8825–8850. https://doi.org/10.1002/2017WR02075260-1364

Lutz, A. F., Immerzeel, W. W., Shrestha, A. B., & Bierkens, M. F. P. (2014). Consistent increase in High Asia's runoff due to increasing glacier melt and precipitation. *Nature Climate Change*, *4*(7), 587–592. https://doi.org/10.1038/nclimate2237

Mantua, N. J., Hare, S. R., Zhang, Y., Wallace, J. M., & Francis, R. C. (1997). A Pacific inter-decadal climate oscillation with impacts on salmon production. *Bulletin of the American Meteorological Society*, *78*(6), 1069–1079. https://doi.org/10.1175/1520-0477(1997)078<1069:APICOW>2.0.CO;2

Marzeion, B., Cogley, J. G., Richter, K., & Parkes, D. (2014). Attribution of global glacier mass loss to anthropogenic and natural causes. *Science*, *345*(6199), 919–921. https://doi.org/10.1126/science.1254702

Minder, J. R., Mote, P. W., & Lundquist, J. D. (2010). Surface temperature lapse rates over complex terrain: Lessons from the Cascade Mountains. *Journal of Geophysical Research*, *115*, D14122. https://doi.org/10.1029/2009JD013493

Moore, R. D., Fleming, S. W., Menounos, B., Wheate, R., Fountain, A., Stahl, K., et al. (2009). Glacier change in western North America: Influences on hydrology, geomorphic hazards and water quality. *Hydrological Processes*, *23*(1), 42–61. https://doi.org/10.1002/hyp.7162

Naz, B. S., Frans, C. D., Clarke, G. K. C., Burns, P., & Lettenmaier, D. P. (2014). Modeling the effect of glacier recession on streamflow response using a coupled glacio-hydrological model. *Hydrology and Earth System Sciences*, *18*(2), 787–802. https://doi.org/10.5194/hess-18-787-2014

Nolin, A. W., Phillippe, J., Jefferson, A., & Lewis, S. L. (2010). Present-day and future contributions of glacier runoff to summertime flows in a Pacific Northwest watershed: Implications for water resources. *Water Resources Research*, *46*, W12509. https://doi.org/10.1029/2009WR008968

Nylen, T. (2004). Spatial and temporal variations of glaciers on Mount Rainier between 1913 and 1994. (Master's thesis, Portland State University)

Ohmura, A. (2011). Observed mass balance of mountain glaciers and Greenland ice sheet in the 20th century and the present trends. *Surveys in Geophysics*, *32*(4–5), 537–554. https://doi.org/10.1007/s10712-011-9124-4

Oyler, J. W., Dobrowski, S. Z., Ballantyne, A. P., Klene, A. E., & Running, S. W. (2015). Artificial amplification of warming trends across the mountains of the western United States. *Geophysical Research Letters*, *42*, 153–161. https://doi.org/10.1002/2014GL062803

Pelto, M. S., & Hedlund, C. (2001). Terminus behavior and response time of North Cascade glaciers, Washington, USA. *Journal of Glaciology*, *47*(158), 497–506. https://doi.org/10.3189/172756501781832098

Rabatel, A., Dedieu, J. P., & Vincent, C. (2016). Spatio-temporal changes in glacier-wide mass balance quantified by optical remote sensing on 30 glaciers in the French Alps for the period 1983–2014. *Journal of Glaciology*, *62*(236), 1153–1166. https://doi.org/10.1017/jog.2016.113

Ragettli, S., Pellicciotti, F., Immerzeel, W. W., Miles, E. S., Petersen, L., Heynen, M., et al. (2015). Unraveling the hydrology of a Himalayan catchment through integration of high resolution in situ data and remote sensing with an advanced simulation model. *Advances in Water Resources*, *78*(2015), 94–111. https://doi.org/10.1016/j.advwatres.2015.01.013

Rasmussen, L. A., & Conway, H. (2001). Estimating South Cascade Glacier (Washington, USA) mass balance from a distant radiosonde and comparison with Blue Glacier. *Journal of Glaciology*, *47*(159), 579–588.

Riedel, J., Wilson, S., Baccus, W., Larrabee, M., Fudge, T., & Fountain, A. (2015). Glacier status and contribution to streamflow in the Olympic Mountains, Washington, USA. *Journal of Glaciology*, *61*(225), 8–16. https://doi.org/10.3189/2015JoG14J138

Riedel, J. L., Larrabee, M. A., 2011a. Mt. Rainier National Park Glacier Mass Balance Monitoring Annual Report, Water Year 2009. North Coast and Cascades Network, National Park Service, Natural Resource Stewardship and Science, Natural Resource Technical Report NPS/NCCN/NRTR-2011/484, Fort Collins, Colorado.

Riedel, J. L., Larrabee, M. A., 2011b. North Cascades National Park Glacier Mass Balance Monitoring Annual Report, Water Year 2009. North Coast and Cascades Network, National Park Service, Natural Resource Stewardship and Science, Natural Resource Technical Report NPS/NCCN/NRTR-2011/483, Fort Collins, Colorado

Rupp, D. E., Abatzoglou, J. T., Hegewisch, K. C., & Mote, P. W. (2013). Evaluation of CMIP5 20th century climate simulations for the Pacific Northwest USA. *Journal of Geophysical Research-Atmospheres*, *118*, 10,884–10,906. https://doi.org/10.1002/jgrd.50843

Rupp, D. E., Abatzoglou, J. T., & Mote, P. W. (2017). Projections of 21st century climate of the Columbia River Basin. *Climate Dynamics*, *49*(5–6), 1783–1799. https://doi.org/10.1007/s00382-016-3418-7

Salathé, E. P., Leung, L. R., Qian, Y., & Zhang, Y. (2010). Regional climate model projections for the State of Washington. *Climatic Change*, *102*(1–2), 51–75. https://doi.org/10.1007/s10584-010-9849-y

Salathé, E. P. Jr., Steed, R., Mass, C. F., & Zahn, P. H. (2008). A high-resolution climate model for the US Pacific Northwest: Mesoscale feedbacks and local responses to climate change. *Journal of Climate*, *21*(21), 5708–5726. https://doi.org/10.1175/2008JCLI2090.1

Saulnier, G. M., Beven, K., & Obled, C. (1997). Including spatially variable effective soil depths in TOPMODEL. *Journal of Hydrology*, *202*(1–4), 158–172. https://doi.org/10.1016/S0022-1694(97)00059-0

Schaefli, B., Hingray, B., & Musy, A. (2007). Climate change and hydropower production in the Swiss Alps: Quantification of potential impacts and related modelling uncertainties. *Hydrology and Earth System Sciences Discussions*, *11*(3), 1191–1205. https://doi.org/10.5194/hess-11-1191-2007

Schaner, N., Voisin, N., Nijssen, B., & Lettenmaier, D. P. (2012). The contribution of glacier melt to streamflow. *Environmental Research Letters*, *7*(3), 034029. https://doi.org/10.1088/1748-9326/7/3/034029

Sen, P. K. (1968). Estimates of the regression coefficient based on Kendall's tau. *Journal of the American Statistical Association*, *63*(324), 1379–1389. https://doi.org/10.1080/01621459.1968.10480934

Shean, D. E., Alexandrov, O., Moratto, Z. M., Smith, B. E., Joughin, I. R., Porter, C., & Morin, P. (2016). An automated, open-source pipeline for mass production of digital elevation models (DEMs) from very-high-resolution commercial stereo satellite imagery. *ISPRS Journal of Photogrammetry and Remote Sensing*, *116*, 101–117. https://doi.org/10.1016/j.isprsjprs.2016.03.012

Spicer R. C. (1986). Glaciers in the Olympic Mountains, Washington: Present distribution and recent variations. (MS thesis, University of Washington)

Stahl, K., & Moore, R. D. (2006). Influence of watershed glacier coverage on summer streamflow in British Columbia, Canada. *Water Resources Research*, *42*, W06201. https://doi.org/10.1029/2006WR005022

Strauch, R., Istanbulluoglu, E., Nudurupati, S. S., Bandaragoda, C., Gasparini, N. M., & Tucker, G. E. (2018). A hydroclimatological approach to predicting regional landslide probability using Landlab. *Earth Surface Dynamics*, *6*(1), 49–75. https://doi.org/10.5194/esurf-6-49-2018

Tangborn, W. V. (1984). Prediction of glacier derived runoff for hydroelectric development. *Geografiska Annaler. Series A, Physical Geography*, *66*(3), 257–265. https://doi.org/10.1080/04353676.1984.11880114

Thornton, P. E., & Running, S. W. (1999). An improved algorithm for estimating incident daily solar radiation from measurements of temperature, humidity, and precipitation. *Agricultural and Forest Meteorology*, *93*(4), 211–228. https://doi.org/10.1016/S0168-1923(98)00126-9

Van Beusekom, A. E., & Viger, R. J. (2016). A glacier runoff extension to the precipitation runoff modeling system. *Journal of Geophysical Research - Earth Surface*, *121*, 2001–2021. https://doi.org/10.1002/2015JF003789

Watanabe, S., Kanae, S., Seto, S., Yeh, P. J. F., Hirabayashi, Y., & Oki, T. (2012). Intercomparison of bias-correction methods for monthly temperature and precipitation simulated by multiple climate models. *Journal of Geophysical Research*, *117*, D23114. https://doi.org/10.1029/2012JD018192

Weiler, M., Seibert, J., & Stahl, K. (2018). Magic components—Why quantifying rain, snowmelt, and icemelt in river discharge is not easy. *Hydrological Processes*, *32*(1), 160–166. https://doi.org/10.1002/hyp.11361

Wigmosta, M. S., Nijssen, B., Storck, P., & Lettenmaier, D. P. (2002). The distributed hydrology soil vegetation model. In V. P. Singh, & D. K. Frevert (Eds.), *Mathematical models of small watershed hydrology and applications*, (pp. 7–42). Littleton, CO.: Water Resource Publications.

Wigmosta, M. S., Vail, L. W., & Lettenmaier, D. P. (1994). A distributed hydrology-vegetation model for complex terrain. *Water Resources Research*, *30*(6), 1665–1679. https://doi.org/10.1029/94WR00436

Woods, R. A. (2009). Analytical model of seasonal climate impacts on snow hydrology: Continuous snowpacks. *Advances in Water Resources*, *32*(10), 1465–1481. https://doi.org/10.1016/j.advwatres.2009.06.011

Yapo, P. O., Gupta, H. V., & Sorooshian, S. (1998). Multi-objective global optimization for hydrologic models. *Journal of hydrology*, *204*(1-4), 83–97.